

Early Neoproterozoic magmatism (1000–910 Ma) of the Zadinian and Mayumbian Groups (Bas-Congo): onset of Rodinia rifting at the western edge of the Congo craton

L. Tack ^{a,*}, M.T.D. Wingate ^b, J.-P. Liégeois ^a, M. Fernandez-Alonso ^a,
A. Deblond ^a

^a *Department of Geology and Mineralogy, Royal Museum for Central Africa (RMCA), 13 Leuvensesteenweg, B-3080 Tervuren, Belgium*

^b *Tectonics Special Research Centre, The University of Western Australia, 35 Stirling Highway, Crawley, WA 6009, Australia*

Abstract

New ion microprobe U–Pb zircon ages, as well as some geochemical and isotopic analyses, for key igneous units within the central part of the West Congo belt are integrated with geological information to provide an updated geological map (1:1000000 scale) and a synthetic type cross-section of the belt, as well as an updated lithostratigraphic chart of the ‘West Congo Supergroup’. Three Neoproterozoic units are recognised, from oldest to youngest, the Zadinian, Mayumbian and West Congolian ‘Groups’. Emplacement of early Zadinian peralkaline granites (Noqui massif, 999 ± 7 Ma) and rhyolites (Palabala) was accompanied by incipient rift sedimentation, corresponding to the onset of transtensional rifting, preferentially in a transverse mega-shear setting along the margin of the Congo craton. Subsequent upper Zadinian magmatism produced a thick (1600–2400 m) basaltic sequence (Gangila), which has geochemical characteristics typical of continental flood basalts (CFBs). The Gangila basalts, associated with major pull-apart rifting, were followed rapidly by the 3000–4000 m thick Mayumbian rhyolitic lavas, dated at 920 ± 8 Ma at the base and 912 ± 7 Ma at the top. The felsic lavas are intruded by coeval high-level (micro)granites, whose emplacement is dated at 924 ± 25 Ma (Mativa body) and at 917 ± 14 Ma (Bata Kimenga body) in the Lufu massif. This voluminous bimodal magmatic province is similar to the Paraná and Deccan provinces, and shares similar lithospheric sources. It corresponds to the initial, transtensional rifting stage along the western edge of the Congo craton before Rodinia breakup. The early Neoproterozoic rocks of the West Congo Supergroup rest unconformably on a ca. 2.1 Ga Palaeoproterozoic polycyclic basement (Kimezian Supergroup). No Mesoproterozoic events are recorded in the area. Following the initial, transtensional early Neoproterozoic (ca. 1000–910 Ma) rifting stage, Bas-Congo behaved as a passive margin of the Congo craton, as indicated by deposition of ca. 4000 m of Neoproterozoic (pre-Pan-African) platform sediments (lower part of West Congolian Group) preceding ca. 2000 m of Pan-African molasse-type sediments (upper part of West Congolian Group). In the late Neoproterozoic, during Pan-African assembly of Gondwanaland, the Bas-Congo passive margin, which was largely protected by thick lithosphere of the Congo craton, collided with a western active margin to form the Brasiliano-Araçuaí belt, now

* Corresponding author. Tel.: +32-2-7695425; fax: +32-2-7695432.

E-mail address: ltack@afRICAMuseum.be (L. Tack).

preserved adjacent to the São Francisco craton of Brazil. This collision, which ended in Bas-Congo at ca. 566 Ma, induced relatively limited effects in the West Congo belt, which experienced no late Neoproterozoic magmatic activity. © 2001 Elsevier Science B.V. All rights reserved.

Keywords: Basalt; Geochemistry; Ion microprobe; Neoproterozoic; Rhyolite; Rodinia; West Congo belt; Zircon

1. Introduction

In the last three decades, the role of the West Congo (or West Congolian) belt in geodynamic modelling of the Pan-African-Brasiliano belts, in particular with respect to Gondwanaland and Rodinia supercontinent reconstructions, has been the subject of episodic discussion (Vellutini et al., 1983; Cahen et al., 1984 and references therein; Byamungu et al., 1987; Boudzoumou and Trompette, 1988; Franssen and André, 1988; Pedrosa-Soares et al., 1992, 1998, 2001; Maurin, 1993; Trompette, 1994, 2000; Unrug, 1996, 1997; Unrug et al., 1996).

The West Congo belt is ca. 1400 km long, 150–300 km wide, and extends subparallel to the Atlantic coast between 1 and 12°S (Fig. 1a and b). Its structure (Figs. 2 and 3) was acquired during the Pan-African orogeny, the final stages of which are best dated at ca. 566 Ma [unpublished Ar–Ar data on greenschist facies rocks from Bas-Congo province in the Democratic Republic of Congo (formerly Zaire), Boven, pers. comm.]. In this paper, we use the term ‘Pan-African’ (in preference to the local term ‘West Congo orogeny’) to refer to orogenic events that occurred between about 800 and 500 Ma.

This paper deals with early Neoproterozoic (ca. 1000–910 Ma) magmatic events, which are poorly

documented in Central Africa, yet are essential for understanding the transition from Rodinia breakup to Gondwanaland assembly. We present new ion microprobe (SHRIMP) U–Pb zircon ages as well as some geochemical and isotopic analyses for key igneous units within the central part of the West Congo belt. We integrate these data with newly revised geological information in an updated geological map (1:1,000,000 scale) and synthetic type cross-section of the entire belt, and discuss implications for the nature and timing of magmatic and tectonic events.

According to IUGS rules for nomenclature of lithostratigraphic units, attributions in this paper to supergroup, group, subgroup and formation differ from all previously proposed lithostratigraphies for the West Congo belt, although regional names have been retained to avoid confusion. Following the example of the recent introduction of the term ‘Katanga Supergroup’ for the Lufilian and northern Zambezi belts in the Democratic Republic of Congo and Zambia (Porada and Berhorst, 2000), the new term ‘West Congo Supergroup’ is adopted in this paper, and includes, from oldest to youngest, the Zadinian, Mayumbian, and West Congolian Groups (see in particular, Section 3 and Fig. 4).

We show that the studied magmatic events mark major rifting of Rodinia on the western

Fig. 1. (a) Geological map of the West Congo Pan-African belt, compiled from geological maps of Gabon (Hudeley and Belmonte, 1966; Bassot, 1988), the Republic of Congo (‘Congo-Brazzaville’; Dadet, 1966; Desthieux, 1992, 1994), Cabinda and Angola (de Carvalho, 1981; de Araújo and Perevalov, 1998; de Araújo et al., 1988), the Democratic Republic of Congo (‘Congo–Kinshasa’; formerly Zaire; Lepersonne, 1974) and the western part of the Bas-Congo province in the Democratic Republic of Congo (Tack, 1975a). Background; hill shaded digital elevation model, based on the global 30 arc-second elevation dataset (GTOPO30) compiled by the United States Geological Survey, EROS Data Centre, in 1996. Structural elements are omitted for legibility of the map but are available on 1:1000000 print copy and are also indicated on (b). Revised and simplified lithostratigraphy, see Fig. 4 and explanations in Section 1 of text. Box, simplified map with several countries, scanned from Tack (1995), Congo–B, Congo–Brazzaville, i.e. Republic of Congo; Congo–K, Congo–Kinshasa (formerly Zaire), i.e. Democratic Republic of Congo. (b) Enlarged view of (a), focussing on the central flexure of the West Congo belt (including Bas-Congo and northern Angola) and emphasising the occurrence of the ‘Noqui’ type peralkaline granitoids, that are restricted to that part of the belt. Revised and simplified lithostratigraphy, see Fig. 4 and explanations in Section 1 of text. Localisation of four cross-sections A–D (Fig. 3a–d) and some relevant locality names are indicated on the map; Ki, Kinshasa; Br, Brazzaville.

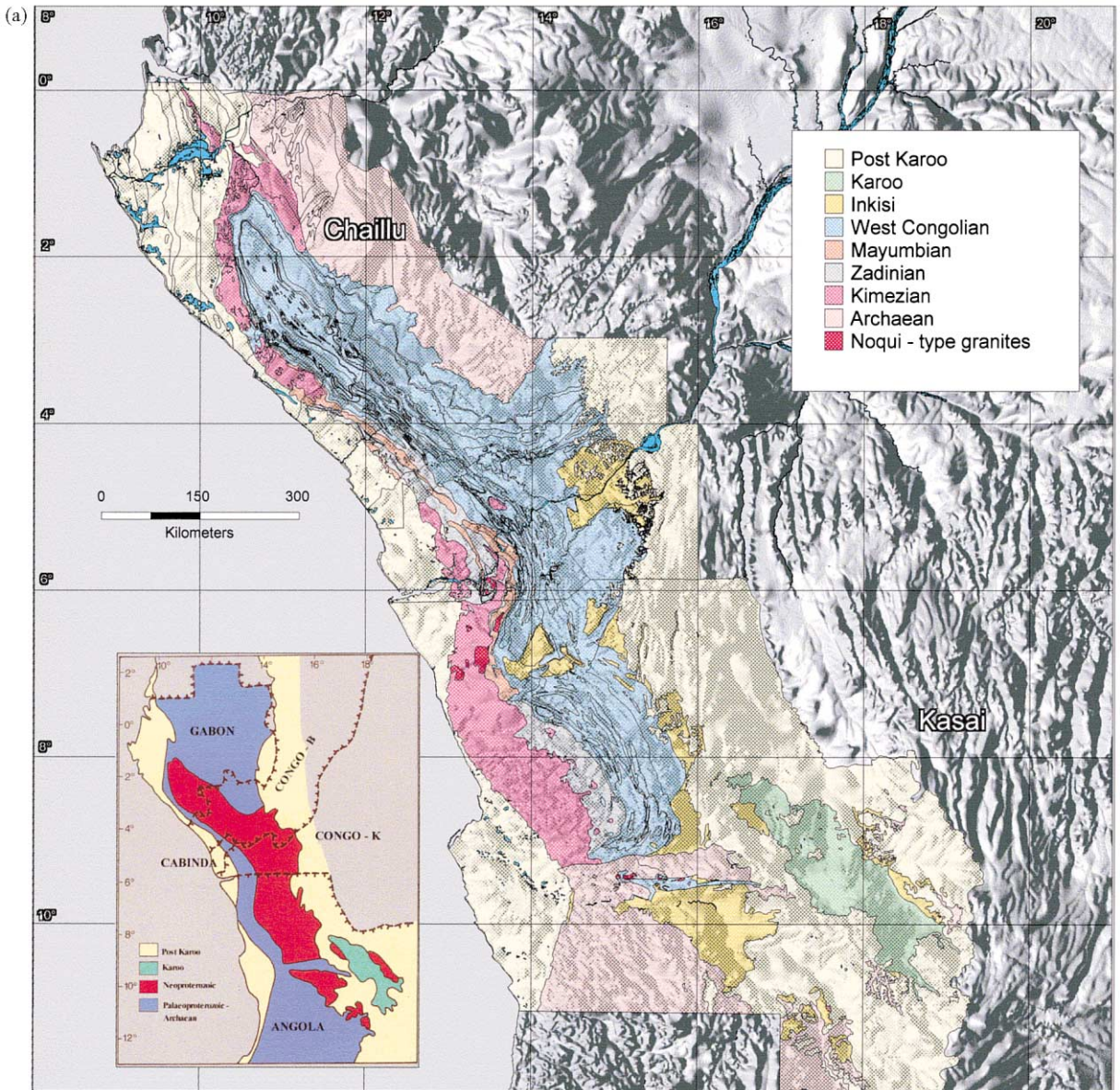


Fig. 1.

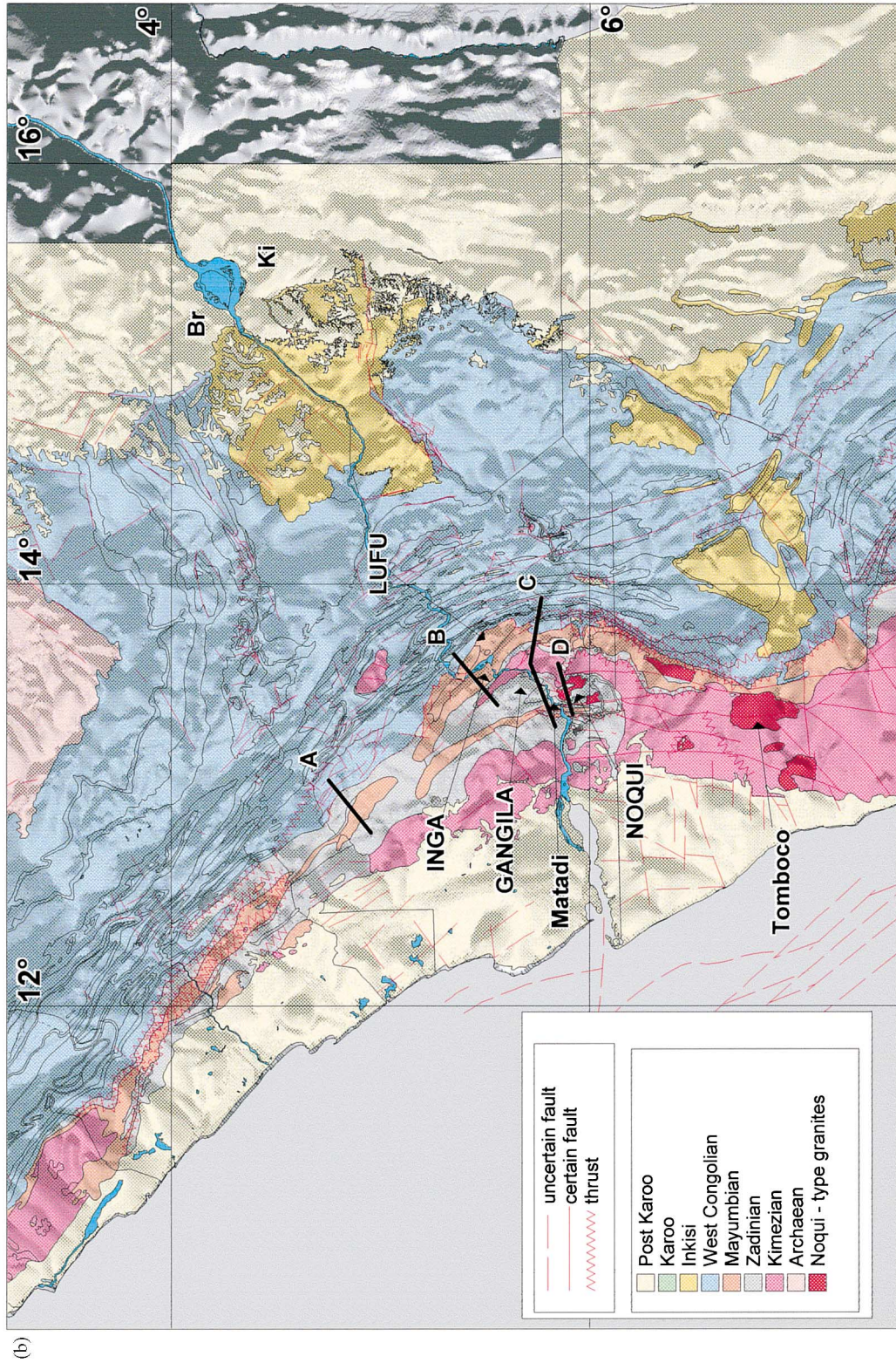


Fig. 1. (Continued)

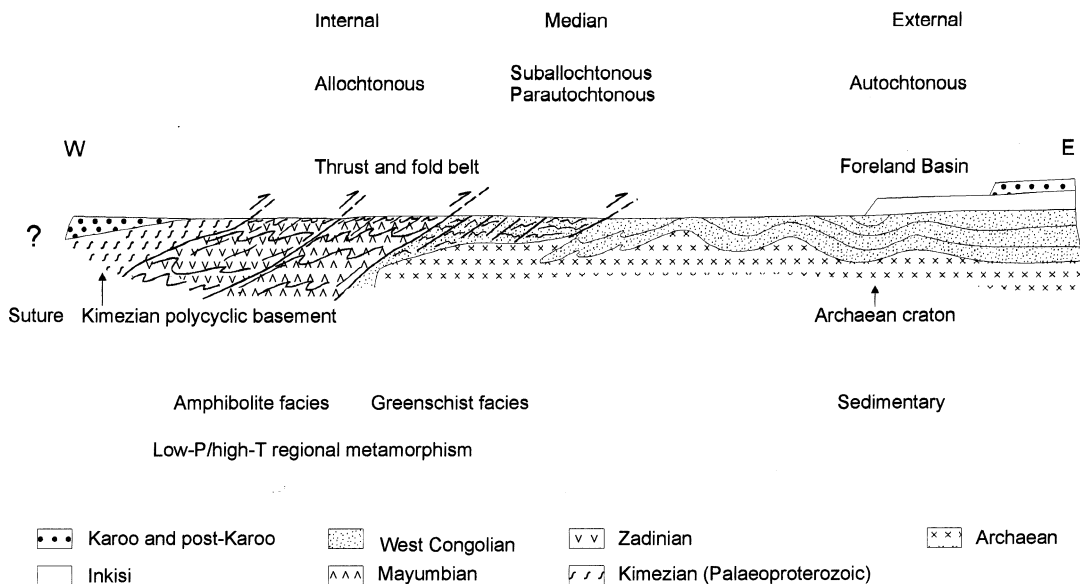


Fig. 2. Synthetic E–W type cross-section of the West Congo Pan-African tectono-metamorphic domains, based on field and gravimetry data. Indicated thrusts have limited displacements. Terminology of envisaged structural and metamorphic domains is after various authors quoted in references. If a Pan-African suture zone exists, it should be located to the west of the studied area [further explanations and references in text, in particular in Tack (1975a), Franssen and André (1988)].

edge of the present-day Congo craton. Evidence of these events has been well preserved during the subsequent Pan-African orogeny because the region suffered only moderate deformation and no magmatism, owing to the proximity to the east of the Archaean Congo craton. In contrast, ophiolitic remnants, high-grade metamorphic rocks and granitoid batholiths occurred farther to the west, and are now preserved in the Araçuaí segment of the Brasiliano belt (Pedrosa-Soares et al., 2001).

2. Structural setting of the West Congo Pan-African tectono-metamorphic domains

An updated synthesis and Geological Information System (GIS)-based geological compilation, at 1:1,000,000 scale, of the entire West Congo belt has recently been completed (Fig. 1a and b; Tack, 1995; Tack and Fernandez-Alonso, 1998; Fernandez-Alonso et al., 2000). The map displays a prominent flexure in its central segment (Bas-Congo province and adjacent northern Angola,

Fig. 1a and b). The area to the northeast of the flexure grades progressively into the foreland of the belt towards the Congo craton. In this area, the main NW–SE trending branches of the Neoproterozoic basin abut the bounding NE-trending ‘Sangha’ aulacogen limited by ‘Combian’ faults (Alvarez and Maurin, 1991; Maurin, 1993, Fig. 1a and b). The area also includes minor pre-Pan-African basement inliers.

Comparison of published cross-sections and lithostratigraphic charts from the countries involved (Fig. 1a and references in Section 1) has enabled construction of a schematic east–west type cross-section of the West Congo tectono-metamorphic domains (Fig. 2), combining field and structural (Tack, 1975a; Boudzoumou and Trompette, 1988; Franssen and André, 1988; Maurin, 1993) as well as gravimetry (Byamungu et al., 1987) data. This type section illustrates a general decrease in deformation and regional metamorphism from west to east.

To the west, in the Pan-African fold-and-thrust belt (Fig. 2), the east-verging, oldest ca. 2.1 Ga Kimezian Supergroup (polycyclic Palaeoproterozoic-

zoic basement) is thrust onto the Zadinian Group, itself in places thrust onto the Mayumbian Group, which finally comes into contact with the youngest West Congolian Group (description of these three Groups is in Section 3). In Bas-Congo (Fig. 1b), a variation in tectonic style is observed from north to south. In the north (Fig. 1b and Fig. 3a), gently-dipping and imbricated thrust slices abound. Further south (Fig. 1b and Fig. 3b), protected to the east by the ‘Lufu’ massif (a large rigid Mayum-

bian granite body), the West Congolian metasedimentary sequences display only upright folding. Moreover, a nonconformity of the West Congolian Group on this Mayumbian granite can be observed only in this part of the West Congo belt (Tack, 1973a, 1975a). This important observation indicates that the West Congolian Group was deposited in situ, after unroofing of the Mayumbian granites, and without subsequent Pan-African thrusting relationships.

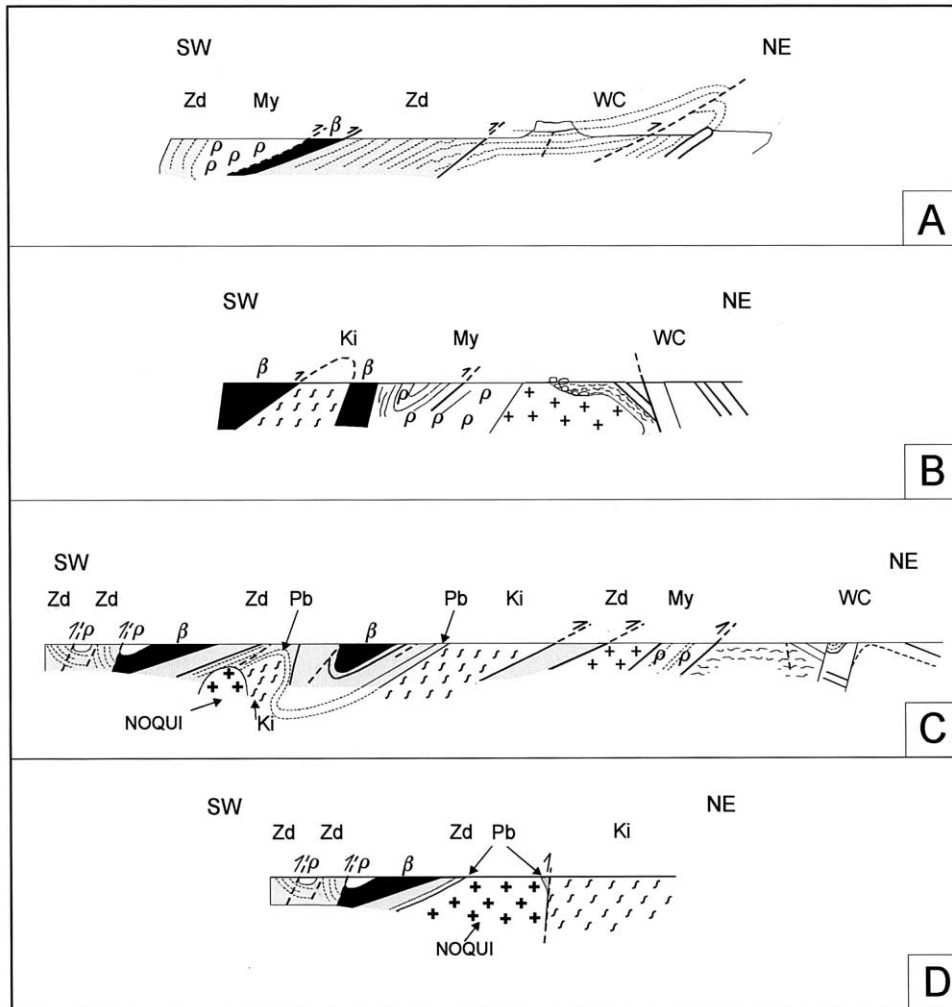


Fig. 3. Four schematic SW–NE cross-sections of the West Congo Pan-African belt in Bas-Congo indicating the observed variation in tectonic style from N to S (explanations in text; see Fig. 1b for locations). Lithostratigraphy (see also Fig. 4 and its legend), Ki, Kimezian Supergroup; Zd, Zadinian Group; My, Mayumbian Group; WC, West Congolian Group; Pb, Palabala Formation. Rock types; β, basalt; ρ, rhyolite; +/+, granite (Mayumbian/Noqui types).

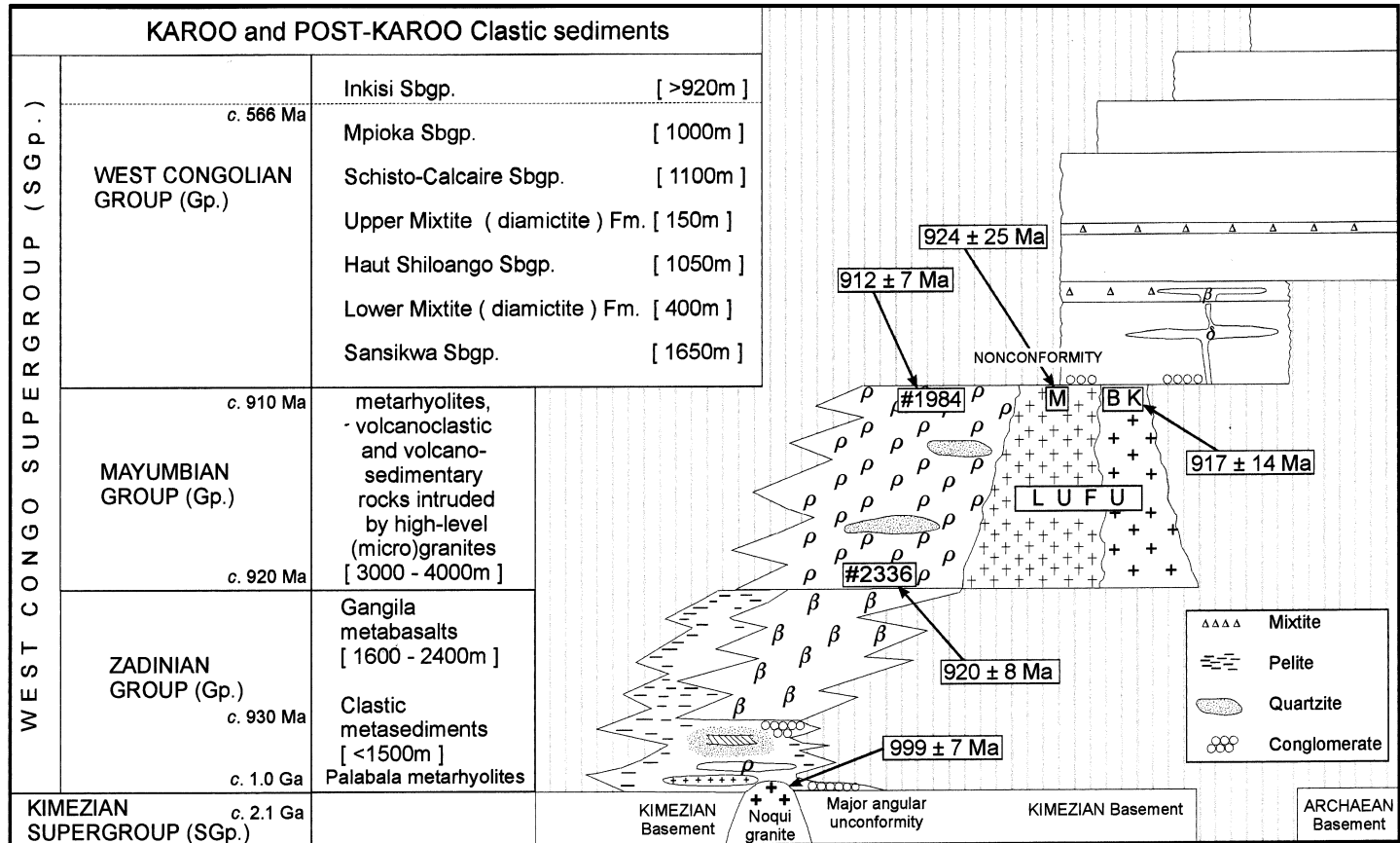


Fig. 4. Lithostratigraphic reconstruction of the ‘West Congo Supergroup’ including the following units, from oldest to youngest, Zadinian, Mayumbian and West Congolian ‘Groups’ with emphasis on the lithology of both the Zadinian and Mayumbian Groups. Moreover, Archaean and Palaeoproterozoic basements as well as Inkisi, Karoo or post-Karoo cover deposits are indicated (explanations in text). According to IUGS rules for nomenclature of lithostratigraphic units, attributions in this paper to supergroup (SGp), group (Gp), subgroup (Sbgp) and formation (Fm) differ from all previously proposed lithostratigraphies for the West Congo belt, although regional names have been retained to avoid confusion. Rock types; β , basalt; ρ , rhyolite; δ , dolerite; M, Mativa; BK, Bata Kimenga.

To the east of the more internal domain, the median, open-fold domain of the West Congolian Group dies out progressively and grades into an external foreland basin, where subtabular sequences of the upper West Congolian Group rest unconformably on the Archaean Congo craton ('Chaillu' and 'Kasai' blocks; Figs. 1 and 2).

Syn-kinematic regional metamorphism, related to Pan-African orogenesis, is of a low pressure–high temperature type (Tack, 1975a,b, 1979a; Franssen and André, 1988), and varies from amphibolite facies, in the west, to greenschist facies and, finally, to unmetamorphosed sedimentary rocks to the east (Fig. 2). Ophiolite remnants and high-grade metamorphic rocks, as well as syn- to post-kinematic granitoid batholiths of Pan-African age, are totally absent throughout the West Congo belt.

Although the internal and median domains of the West Congo belt have suffered thrusting in some areas, displacements of slices along thrust faults may be considered to be of limited amplitude in Bas-Congo (Lepersonne, 1969; Tack, 1975a; Franssen and André, 1988). Nevertheless, Pan-African deformation locally includes strongly developed L–S fabrics and mylonitic corridors. From the section, and because of limited displacement along thrust faults, a lithostratigraphic column for the entire West Congo belt can be constructed (Fig. 4). The column shows the major angular unconformity between the Palaeoproterozoic Kimezian basement and overlying igneous and metasedimentary rocks of the very thick (ca. 5000–6000 m) Zadinian and Mayumbian Groups, as well as the importance of subsequent passive margin sedimentation that characterises the lower part of the overlying West Congolian Group (from Sansikwa to Schisto-Calcaire Subgroups).

3. Lithostratigraphy

Excluding Karoo and younger cover deposits and Palaeoproterozoic (in the west) to Archaean (in the east) basement, the revised reference lithostratigraphic column for the West Congo Supergroup includes, from oldest to youngest, the Zadinian, Mayumbian and West Congolian Groups (Section 1 and Fig. 4).

3.1. The Zadinian Group

The lower part of the Zadinian Group (Tack, 1975a,b; Cahen et al., 1984 and references therein) is composed of continental, siliciclastic metasediments (including black shales), not exceeding 1500 m in thickness, that exhibit strong lateral and vertical facies variations (Fig. 4), consistent with a continental rift environment. In Bas-Congo, these sedimentary rocks are overlain by a 1600–2400 m thick succession of mafic rocks, described under various local names ('Gangila' metabasalts, in type area; Fig. 1b) as predominantly continental flows ('plateau basalts'?, Tack, 1975a,b, 1979b,c). The Zadinian succession, including the Gangila basalts at the top, is overlain concordantly by the Mayumbian Group, which has quite distinct lithology (see Section 3.2). The Gangila basalts are tholeiitic and display, up-section, a slight evolutionary trend (Tack, 1975a,b).

In the central segment of the West Congo belt, a major angular unconformity separates the Zadinian Group from the underlying ca. 2.1 Ga polycyclic Palaeoproterozoic basement (Kimezian Supergroup, including mainly gneisses, migmatites, and amphibolites; Delhal and Ledent, 1976; Vellutini et al., 1983; Cahen et al., 1984 and references therein; Boudzoumou and Trompette, 1988; Maurin et al., 1990; Djama et al., 1992). Both to the north and to the south of the Bas-Congo province, the basaltic activity was much less. In the Republic of Congo, we consider amphibolitic lenses (Vicat and Vellutini, 1987, 1988; Kampunzu et al., 1991) interbedded in the 'Bikossi' metaquartzites as limited lateral equivalents of the Gangila basalts.

In the Matadi area of Bas-Congo (Fig. 1b), the base of the Zadinian Group is represented by the Palabala Formation (500 m, Lepersonne, 1969; Steenstra, 1973), which is composed mainly of quartzite and biotite schist with minor conglomerate. Towards the top of the formation, metarhyolite is intercalated (Franssen and André, 1988). The lower part of this formation, as well as the underlying older Palaeoproterozoic (Kimezian) basement, is intruded by many sills of rhyolite.

South of Matadi, the peralkaline 'Noqui' granite is exposed in the central segment of the West

Congo belt (Fig. 1a and b and Fig. 3c and d), adjacent to large areas of Palaeoproterozoic basement (Kimezian Supergroup). Cogenetic peralkaline microgranite intrudes the Palabala Formation along the northern border of the Noqui massif. The rhyolite sills and flows of the Palabala Formation outcrop in the vicinity of these microgranites. The field setting of the ‘Noqui’ granite is contentious (Cahen et al., 1976, 1984), and some arguments point to a ‘post-tectonic’ (i.e. post-Pan-African) character (Franssen and André, 1988), whereas others suggest a ‘pre-tectonic’ setting (Delhal et al., 1971 and references therein; Korpershoek, 1964a,b).

Proximity of the Palabala rhyolitic sills and flows to the Noqui massif and cogenetic microgranites, the identical geochemical signatures of these effusive and intrusive rocks (Franssen and André, 1988), and the absence of any peralkaline intrusive rocks in the overlying ‘Matadi’ quartzites and Gangila basalts of the Zadinian Group, corroborate the development of an early Zadinian phase of volcanic–plutonic peralkaline magmatism in association with incipient rift-type sedimentation.

To the south of Noqui, similar peralkaline granitoids (e.g. ‘Tomboco’ massif; Fig. 1a and b) are exposed in northern Angola (Korpershoek, 1964a,b). Their occurrence is restricted to the central zone of the West Congo belt. In this peculiar structural and rheological setting (including abundance of Palaeoproterozoic ‘Kimezian’ basement), the Zadinian Group and peralkaline granitoids have suffered only moderately from Pan-African deformation and metamorphism (Fig. 1b and Fig. 3c and d).

3.2. The Mayumbian Group

The Mayumbian Group (Tack, 1975a, 1979a, 1983; Cahen et al., 1984 and references therein) is a felsic volcanic–plutonic sequence with subordinate volcano-sedimentary and sedimentary intercalations. Its internal lithostratigraphy varies strongly from place to place; hence, detailed stratigraphic correlations are difficult. In Bas-Congo, the 3000–4000 m thick, predominantly felsic, volcanic sequence described under various

local names (‘Inga’ metarhyolites, in type area; Fig. 1b; Steenstra, 1973; Tack, 1975a, 1979a) is intruded by a suite of successively emplaced high-level granitic bodies with various local names and generally referred to as the ‘Lufu’ massif (Fig. 1b; Tack, 1973a,b, 1979a).

Field and petrographic characteristics of the Mayumbian rocks in Bas-Congo have been described in detail by Tack (1973a,b, 1975a, 1979a). In the Lufu massif and adjacent areas of the Inga felsic lavas, the volcanic–plutonic character of the succession is illustrated by ubiquitous bluish, high-temperature, euhedral though embayed, ‘rhyolitic’ quartz phenocrysts in the various rock types. In the case of the Lufu massif, an excellent correlation is found between the relative chronology of emplacement of the successive intrusive bodies (as established by field evidence, i.e. relationships of dykes and enclaves), petrography and preliminary geochemical investigation showing rock compositions ranging from monzogranite via abundant syenogranite (e.g. ‘Mativa’ body) to subordinate alkali feldspar granite (e.g. ‘Bata Kimga’ body, Tack, 1973a, 1975a, 1979a).

In mylonitic corridors (see Section 2), the Mayumbian rocks were strongly deformed during Pan-African orogenesis. To the south, in Angola, they include the ‘Lufico’ gneiss (Korpershoek, 1964a,b) and in the north they extend into the Republic of Congo and Gabon as the ‘Loukoula’ and/or ‘Kakamoeka’ metarhyolites, and the ‘Mfoubou’ and ‘Kanda’ granites (Maurin et al., 1991; Djama et al., 1992; Vicat et al., 1992).

3.3. The West Congolian Group

The internal lithostratigraphy of the West Congolian Group in Bas-Congo has been discussed in detail by Cahen (1978), Cahen et al. (1984). It comprises two main sedimentary successions: pre-Pan-African passive-margin platform sequences (from Sansikwa to Schisto-Calcaire Subgroups; ca. 4000 m thick) and late- to post-Pan-African molasse sequences (Mpioka and Inkisi Subgroups; ca. 2000 m thick; Fig. 4).

The passive margin sequences include both siliclastic and carbonate rocks (with local stromatolites) and two horizons of diamictite, the lower

one being associated with an undated basaltic episode ('Kimbungu' pillow lavas and 'Sumbi' feeder dolerite sills and dykes with tholeiitic affinity; De Paepe et al., 1975; Kampunzu et al., 1991; Mpemba Boni and Vellutini, 1992). The lowermost Sansikwa Subgroup rests nonconformably on the Lufu granites (see Section 2; Fig. 3b). The emplacement age of the granites (see below) thus provides an older limit for the onset of deposition of the West Congolian Group. In adjacent Popular Republic of Congo, a model of carbonate ramp development associated with biological activity, based on modern sequence stratigraphy and sedimentological studies has been proposed for the Schisto-Calcaire Subgroup basin evolution (Alvarez, 1995; Alvarez and Maurin, 1991).

The molasse sequences (Fig. 4) are foreland basin deposits with predominantly 'red bed' facies. Their depositional age, although poorly constrained and beyond the scope of this paper, is bracketed between late Neoproterozoic and pre-Karoo times. The Mpioka Subgroup corresponds to the molasse of the West Congo belt (Alvarez and Maurin, 1991), occurs all along its length, and is locally even slightly deformed; as such, it is a late marker of the evolution of the West Congo belt. The overlying tabular Inkisi Subgroup is post-Pan-African (Alvarez et al., 1995) and its deposition area is unrelated to the West Congo belt trend and evolution. In Angola, the Inkisi Subgroup is overlain by Karoo deposits and, therefore, must be older than Permian, as proposed by Alvarez et al. (1995), but still belong to the Palaeozoic, being a foreland-basin deposit unrelated to and younger than the Pan-African orogeny. For this reason, the Inkisi Subgroup (in contrast with previous papers) has been separated from the West Congolian Group and considered as an individual lithostratigraphic unit (Fig. 1a and b and Figs. 2 and 4).

4. U–Pb zircon SHRIMP geochronology

4.1. Noqui peralkaline granite (RG71.299)

The petrography of Noqui granite sample RG71.299 and the characteristics of its zircons

were described by Delhal et al. (1971) and Cahen et al. (1976). The sample is a medium- to coarse-grained riebeckite granite, containing minor aegirine and biotite. Zircons are associated mainly with ferromagnesian minerals, and are equant, sub- to euhedral, and exhibit bipyramidal forms. They are typically 150–200 μm in length, variably cracked, and some exhibit step-like faces. The zircons are light to dark brown, range from transparent to opaque, and concentric euhedral zoning is common in transmitted light. A very small proportion of zircons in the sample ($\ll 1\%$) are colourless and transparent. A representative selection of > 100 zircons containing transparent and apparently undamaged areas was mounted for U–Pb analysis. Ion microprobe U–Pb analytical methods are described in the Appendix A.1. Data were collected in sets of six scans during a single analytical session and are listed in Table 1.

High and variable common Pb in Noqui zircons was noted previously (Delhal et al., 1971; Cahen et al., 1976). The first scans of many zircons indicated extremely high contents of ^{204}Pb , and most analyses of these crystals were terminated without collecting data. Useful data were obtained for 16 zircons, including two of the colourless variety. Uranium concentration varies from 40 to 1040 ppm, with a mean of 600 ppm; $^{232}\text{Th}/^{238}\text{U}$ ratios range from 0.2 to 1.0, and average 0.4. Estimated using ^{204}Pb , the proportion of common ^{206}Pb in measured ^{206}Pb (f_{206} in Table 1) is less than 0.5% for 8 of 16 analyses (those with uncorrected compositions close to concordia), and varies between 1.1 and 15% for the other eight analyses (those dispersed above concordia in Fig. 5a).

After correction for common Pb using ^{204}Pb , most analyses are within error of concordia; some dispersion to the right in Fig. 5a may be the result of having analysed areas of zircon that have lost Pb. The $^{206}\text{Pb}^*/^{238}\text{U}$ ages (Pb* denotes radiogenic Pb) exhibit a prominent peak (Fig. 5b) at 999 ± 7 Ma (95% confidence interval), calculated using maximum-likelihood mixture-modelling (Sambridge and Compston, 1994). Corresponding $^{207}\text{Pb}^*/^{206}\text{Pb}^*$ ages, although much less precise, show a prominent peak at 990 Ma. The two colourless zircons analysed (1.1 and 7.1) yielded

Table 1
Ion microprobe U–Pb zircon data for Noqui granite sample RG71.299

Grain area	^{238}U (ppm)	Th/U	f_{206} (%)	$^{207}\text{Pb}^*/^{206}\text{Pb}^*$		$^{206}\text{Pb}^*/^{238}\text{U}$		$^{206}\text{Pb}^*/^{238}\text{U}$ Age	
				($\pm 1\sigma$)	($\pm 1\sigma$)	(Ma)	($\pm 1\sigma$)		
1.1	202	0.73	0.180	0.06740	0.00128	0.16433	0.00279	980.8	15.5
2.1	1037	0.50	0.316	0.07113	0.00076	0.16776	0.00111	999.8	6.2
3.1	756	0.36	0.308	0.07178	0.00095	0.16961	0.00137	1010.0	7.6
4.1	923	0.56	1.446	0.07278	0.00118	0.16571	0.00102	988.5	5.6
5.1	447	0.21	0.211	0.07013	0.00111	0.16042	0.00168	959.1	9.3
6.1	1017	0.25	1.115	0.07354	0.00121	0.16729	0.00140	997.1	7.7
7.1	41	1.03	0.017	0.07481	0.00347	0.15602	0.00392	934.6	21.9
8.1	377	0.29	1.095	0.07176	0.00205	0.17874	0.00212	1060.0	11.6
10.1	549	0.29	15.05	0.08551	0.00394	0.16272	0.00131	971.9	7.3
11.1	727	0.31	15.02	0.13059	0.00500	0.18753	0.00229	1108.0	12.4
12.1	579	0.38	0.033	0.07313	0.00119	0.16363	0.00140	976.9	7.8
13.1	631	0.43	10.37	0.08385	0.00364	0.18210	0.00195	1078.4	10.6
14.1	951	0.34	3.116	0.08083	0.00297	0.17112	0.00184	1018.3	10.1
15.1	560	0.34	0.434	0.07479	0.00129	0.16756	0.00187	998.7	10.3
16.1	535	0.37	6.007	0.07931	0.00376	0.16791	0.00191	1000.6	10.6
17.1	463	0.50	0.114	0.07154	0.00084	0.16133	0.00131	964.2	7.3

f_{206} is the proportion of common ^{206}Pb in measured ^{206}Pb , estimated using ^{204}Pb . Pb^* indicates radiogenic Pb.

$^{238}\text{U}/^{206}\text{Pb}^*$ ages of 981 and 935 Ma, and have the lowest ^{238}U contents (220 and 40 ppm, respectively), suggesting that their lack of colour reflects a lesser degree of radiation damage than the other zircons in the sample.

Analyses with the highest common Pb are dispersed above concordia, suggesting that common Pb has been underestimated for these analyses. Three (8.1, 11.1, 13.1 in Fig. 5) yield $^{206}\text{Pb}^*/^{238}\text{U}$ ages significantly older than the main group. These crystals are similar in appearance to most other zircons in the sample and hence are unlikely to be xenocrysts. Analyses 11.1 and 13.1 are strongly discordant, indicate 15 and 10% common ^{206}Pb , respectively, and are not considered reliable. Analysis 8.1 yields a $^{206}\text{Pb}^*/^{238}\text{U}$ age of 1060 Ma, although its $^{207}\text{Pb}^*/^{206}\text{Pb}^*$ age is 980 Ma, which is identical to analyses in the main group. It is reasonable to consider that the event responsible for introduction of high common Pb also had some effect on radiogenic $^{206}\text{Pb}^*/^{238}\text{U}$ ratios in these three zircons. Although other explanations are possible, further discussion is beyond the scope of this paper.

Crystallisation ages of the zircons can be estimated by another method, without explicit correction for common Pb. If the Pb in the zircons is a mixture of common and radiogenic Pb, then the analyses will lie (by amounts proportional to their common Pb contents) along a mixing line between initial Pb, at $\text{U}/\text{Pb} = 0$, and radiogenic Pb, on concordia. All zircons of the same age will lie within error of a single regression line through the data, anchored at initial Pb (initial $^{207}\text{Pb}/^{206}\text{Pb} = 0.927$ at 1000 Ma; Cumming and Richards, 1975); data falling significantly to the left of the mixing line suggest the presence of xenocrystic zircons (although see above), whereas dispersion to the right indicates Pb loss. A regression through the Noqui zircon data, excluding those analyses whose individual uncertainties place them more than two standard deviations from the line, yields a concordia intercept of 998 ± 6 Ma (Fig. 5c), identical to the main peak of 999 ± 7 Ma indicated by the 204-corrected $^{238}\text{U}/^{206}\text{Pb}^*$ ages. Because the larger uncertainty of the latter age encompasses the precision of both determinations, 999 ± 7 Ma (95% confidence interval) is consid-

ered to be the most reliable estimate of the crystallisation age of the Noqui granite.

4.2. Mayumbian rhyolites (# 1984 and # 2336)

The petrography of Mayumbian rhyolites has been described by Tack (1979a). Sample # 1984 is from the stratigraphic top of the Mayumbian felsic volcanic sequence, and sample # 2336 is from the base. Sample # 1984 is fine-grained, and contains ~15% mm-scale feldspar crystals and crystal fragments, and ca. 3% phenocrysts of bluish quartz. Sample # 2336 is similar, but contains ca. 10% bluish quartz phenocrysts and 1–2% feldspar crystals. Several hundred zircons were separated from each sample. The least magnetic fraction (1.5 A, 5° side tilt) in each case was mounted for U–Pb analysis. Data for the two samples were collected in sets of six scans during a single analytical session. Results are illustrated in Fig. 6a and b and listed in Table 2. A third

sample, # 58, from approximately the middle of the felsic volcanic sequence, yielded about 15 very small, rounded to spherical zircons, which were identified as probable xenocrysts. Two of the larger crystals from sample # 58 were analysed and yielded concordant ages of 1977 and 1787 Ma (Table 2).

Zircons from sample # 2336 are colourless, euhedral, range up to 300 µm in length, and have length to width ratios between 2:1 and 5:1. Some contain irregular to acicular cavities or inclusions. The best areas of 19 crystals, free of any cracks or inclusions, were selected for analysis. Concentrations of ^{238}U in # 2336 zircons range from 60 to 150 ppm, averaging 100 ppm; Th/U ratios range from 1.0 to 1.5. Values of f_{206} are less than 0.43% for all but one analysis, and the median is 0.09%. Most analyses of sample # 2336 zircons are well grouped and concordant, and yield a mean $^{206}\text{Pb}^*/^{238}\text{U}$ ratio for 18 analyses of 0.15346 ± 0.00058 (MSWD = 0.6), equivalent to

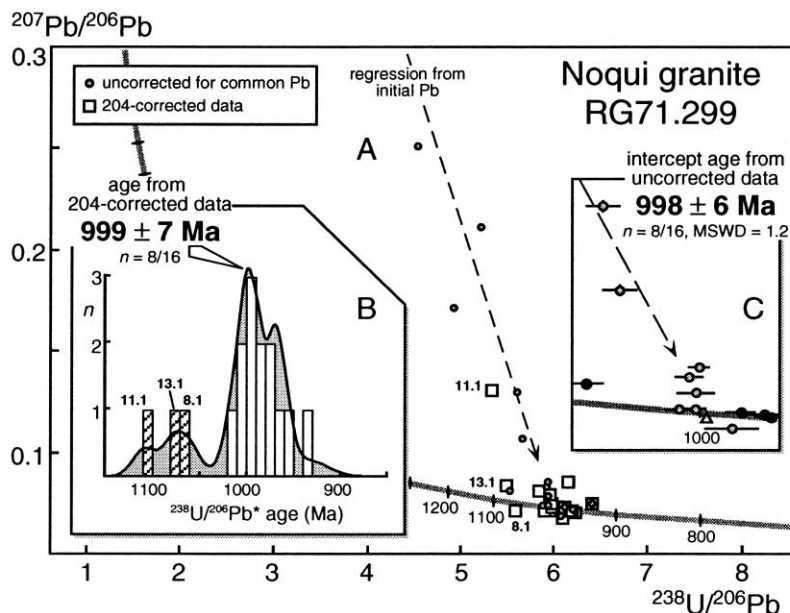


Fig. 5. Ion microprobe analytical data for 16 zircons from Noqui granite sample RG71.299. (a) U–Pb evolution (concordia) diagram showing data uncorrected for common Pb (circles) and corrected using ^{204}Pb (squares). (b) Histogram and probability density plot of ^{204}Pb -corrected $^{238}\text{U}/^{206}\text{Pb}^*$ ages; the age of the main peak/total analyses was determined by mixture-modelling (Sambridge and Compston, 1994). n is the number of analyses contained in the main peak/total analyses. (c) Detail of two-error regression, anchored at common Pb, through data uncorrected for common Pb. Data not used in the regression are shown by black circles. Pb^* indicates radiogenic Pb; error bars are 1σ ; n is the number of analyses used in the regression/total analyses.

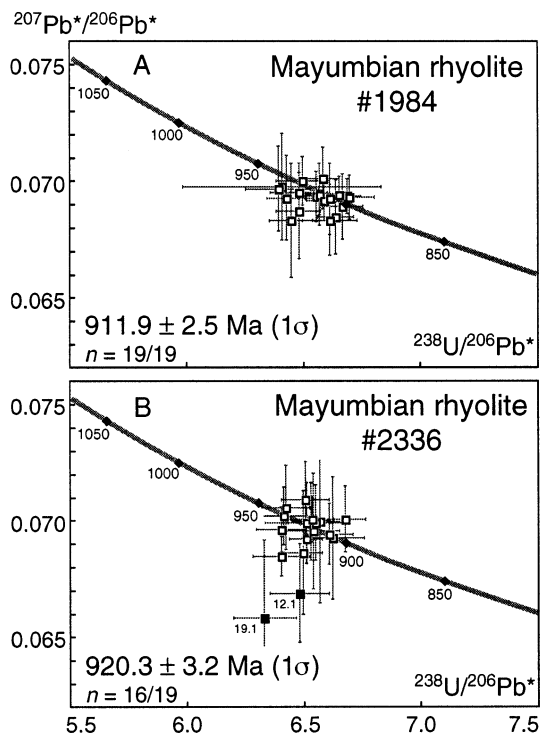


Fig. 6. U–Pb evolution (concordia) diagrams illustrating ion microprobe analytical data for Mayumbian rhyolite samples # 1984 and # 2336. Data are corrected for common Pb using ^{204}Pb . Pb^* indicates radiogenic Pb; error bars and mean ages are 1σ ; n is the number of analyses used in weighted mean/total analyses.

$920.3 \pm 3.2 \text{ Ma}$ (1σ). One analysis (14.1 in Table 2) yielded abnormally low count-rates, indicating that tuning of the secondary ion optics was not optimised correctly, and is excluded. Ratios of $^{207}\text{Pb}^*/^{206}\text{Pb}^*$ are also well grouped, except for abnormally low and relatively imprecise results for two analyses (12.1 and 19.1 in Fig. 6b). These two analyses have the highest values of f_{206} , and may be over-corrected slightly for common Pb. The mean $^{207}\text{Pb}^*/^{206}\text{Pb}^*$ ratio for the remaining 16 analyses is 0.069594 ± 0.00034 (MSWD = 0.3), equivalent to $916.4 \pm 10.2 \text{ Ma}$ (1σ), and does not change significantly if the two outlying analyses are included.

Zircons from sample # 1984 are similar in character to those from sample # 2336, but range up to $450 \mu\text{m}$, and have length to width ratios between 2:1 and 4:1. Nineteen crystals were

analysed. Uranium concentrations in sample # 1984 zircons range from 90 to 450 ppm, averaging 180 ppm, and Th/U ratios range from 0.4 to 1.0. Values of f_{206} are less than 0.33%, with a median of 0.09%. Ratios of $^{206}\text{Pb}^*/^{238}\text{U}$ and $^{207}\text{Pb}^*/^{206}\text{Pb}^*$ are concordant and agree to within analytical precision. The weighted mean $^{206}\text{Pb}^*/^{238}\text{U}$ ratio for 19 analyses is 0.15196 ± 0.00044 (MSWD = 0.9), equivalent to an age of $911.9 \pm 2.5 \text{ Ma}$ (1σ); the mean $^{207}\text{Pb}^*/^{206}\text{Pb}^*$ ratio is 0.069331 ± 0.00026 (MSWD = 0.1), corresponding to $908.6 \pm 7.8 \text{ Ma}$ (1σ).

Although $^{206}\text{Pb}^*/^{238}\text{U}$ and $^{207}\text{Pb}^*/^{206}\text{Pb}^*$ results within each sample are not significantly different from each other, the $^{206}\text{Pb}^*/^{238}\text{U}$ ratios are determined with higher precision, and provide the better estimates of age. The best estimates of ‘absolute’ age are $912 \pm 7 \text{ Ma}$ for sample # 1984 (stratigraphic top of rhyolites), and $920 \pm 8 \text{ Ma}$ for sample # 2336 (stratigraphic base of rhyolites, both 95% confidence limits).

4.3. Mayumbian granites (RG117.805 and # 1027)

The petrography of Mayumbian granites has been described by Tack (1979a). Mativa granite sample RG117.805 is a porphyritic coarse-grained biotite syenogranite, including euhedral though embayed bluish quartz phenocrysts and accessory apatite, zircon, sphene and opaques. Bata Kimenga granite sample # 1027 is a medium- to coarse-grained biotite alkali feldspar granite, including euhedral though embayed bluish quartz phenocrysts and accessory apatite, zircon and opaques. Zircons in the two granites are similar in character, and similar also to those recovered from the Mayumbian rhyolite samples. Most are colourless, euhedral, range up to $400 \mu\text{m}$ in length, and have length to width ratios up to 3:1. Most zircons contain ovoid to acicular cavities, and some from sample RG117.805 are yellowish and turbid (none of this variety was analysed). Zircons from both samples were analysed during the same session; results are illustrated in Fig. 7a and b and listed in Table 3.

For Mativa granite sample RG117.805 (= sample 866; Table 4), 17 analyses were conducted of

17 zircons. Uranium concentrations range from 80 to 240 ppm, with a mean of 150 ppm; Th/U ratios range from 0.3 to 0.9, and average 0.7.

Common Pb content is low; values for f_{206} are less than 0.5%, with a median of 0.04%. All analyses are concordant within relatively large

Table 2

Ion microprobe U–Pb zircon data for Mayumbian rhyolite samples # 1984 and # 2336

Grain area	^{238}U (ppm)	Th/U	f_{206} (%)	$^{207}\text{Pb}^*/^{206}\text{Pb}^*$		$^{206}\text{Pb}^*/^{238}\text{U}$		$^{206}\text{Pb}^*/^{238}\text{U}$ Age	
				($\pm 1\sigma$)		($\pm 1\sigma$)		(Ma)	($\pm 1\sigma$)
<i>Sample # 1984 (& # 58)</i>									
1.1	94	0.54	0.227	0.06976	0.00229	0.15602	0.01034	934.6	57.7
2.1	132	0.73	0.099	0.06966	0.00181	0.15645	0.00342	937.0	19.1
3.1	341	0.69	0.140	0.06939	0.00082	0.15036	0.00146	903.0	8.2
4.1	164	0.52	0.326	0.06844	0.00159	0.15069	0.00180	904.8	10.1
5.1	197	0.71	0.028	0.06923	0.00152	0.15126	0.00227	908.0	12.7
6.1	144	0.84	0.017	0.07001	0.00104	0.15391	0.00267	922.9	14.9
7.1	91	0.60	0.327	0.06870	0.00205	0.15434	0.00229	925.2	12.8
8.1	101	0.51	0.017	0.06948	0.00088	0.15427	0.00291	924.9	16.2
9.1	145	0.94	0.139	0.06833	0.00151	0.15124	0.00268	907.9	15.0
10.1	93	0.56	0.279	0.06828	0.00243	0.15515	0.00225	929.8	12.6
11.1	452	0.82	0.098	0.06936	0.00075	0.14961	0.00137	898.8	7.7
12.1	154	0.96	0.092	0.06891	0.00139	0.15007	0.00208	901.3	11.7
13.1	270	0.81	0.038	0.06934	0.00107	0.15256	0.00113	915.3	6.3
14.1	162	0.68	0.019	0.06927	0.00180	0.15565	0.00200	932.5	11.1
15.1	125	0.61	0.114	0.06943	0.00133	0.15224	0.00209	913.5	11.7
16.1	210	0.43	0.079	0.06929	0.00094	0.14934	0.00240	897.3	13.4
17.1	240	0.87	0.029	0.06938	0.00083	0.15221	0.00152	913.3	8.5
18.1	107	0.67	0.017	0.06915	0.00082	0.15180	0.00169	911.0	9.5
19.1	159	0.59	0.007	0.07012	0.00132	0.15190	0.00154	911.6	8.6
58-1.1	279	0.61	0.051	0.12163	0.00105	0.35807	0.00356	1973.0	16.9
58-2.1	223	0.93	0.063	0.10961	0.00092	0.31876	0.00466	1783.7	22.8
<i>Sample # 2336</i>									
1.1	72	1.18	0.017	0.06962	0.00096	0.15617	0.00258	935.5	14.4
2.1	93	1.33	0.311	0.06861	0.00266	0.15393	0.00198	922.9	11.1
3.1	66	1.03	0.214	0.06957	0.00248	0.15291	0.00266	917.2	14.9
4.1	106	1.22	0.017	0.06844	0.00084	0.15619	0.00298	935.6	16.6
5.1	104	1.23	0.109	0.06989	0.00174	0.15366	0.00409	921.5	22.9
6.1	61	1.48	0.017	0.06942	0.00131	0.15138	0.00240	908.7	13.4
7.1	65	1.08	0.183	0.06997	0.00348	0.15227	0.00267	913.7	14.9
8.1	97	0.99	0.168	0.06991	0.00161	0.15265	0.00280	915.8	15.6
9.1	86	1.35	0.017	0.07005	0.00098	0.15307	0.00219	918.2	12.2
10.1	135	1.26	0.075	0.06998	0.00168	0.15315	0.00199	918.6	11.1
11.1	82	1.06	0.017	0.07020	0.00123	0.15593	0.00290	934.1	16.2
12.1	84	1.22	0.434	0.06689	0.00211	0.15434	0.00301	925.2	16.8
13.1	150	1.23	0.038	0.07006	0.00141	0.14982	0.00197	899.9	11.1
14.1	118	1.37	0.426	0.06668	0.00329	0.16265	0.00420	971.5	23.3
15.1	66	1.39	0.017	0.07056	0.00181	0.15570	0.00252	932.8	14.1
16.1	111	1.30	0.297	0.06926	0.00264	0.15095	0.00304	906.3	17.0
17.1	151	1.17	0.017	0.06920	0.00104	0.15363	0.00167	921.3	9.3
18.1	125	1.17	0.346	0.07088	0.00166	0.15372	0.00246	921.8	13.7
19.1	65	1.16	0.971	0.06582	0.00335	0.15796	0.00337	945.4	18.7

f_{206} is the proportion of common ^{206}Pb in measured ^{206}Pb , estimated using ^{204}Pb . Analyses prefixed by 58- are xenocrystic zircons from sample # 58, as described in the text. Pb* indicates radiogenic Pb.

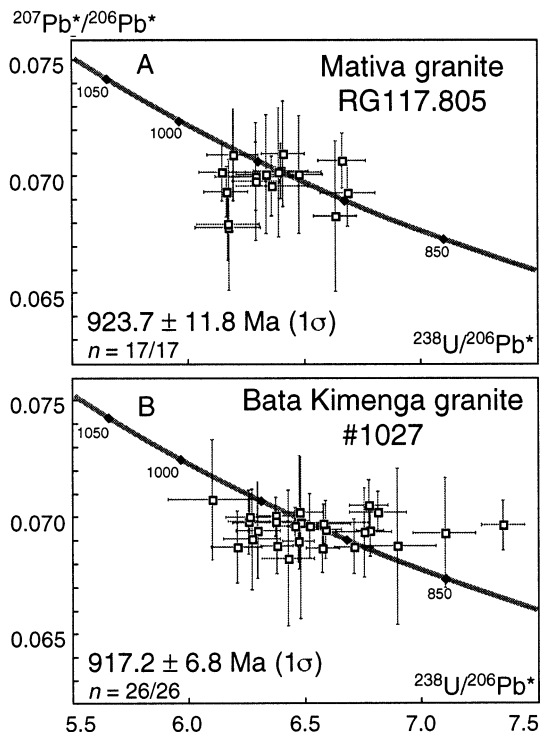


Fig. 7. U–Pb evolution (concordia) diagrams illustrating ion microprobe analytical data for Mayumbian granite samples RG117.805 and #1027. Data are corrected for common Pb using ^{204}Pb . Pb^* indicates radiogenic Pb; error bars and mean ages are 1σ ; n is the number of analyses used in weighted mean/total analyses.

errors. Although one analysis (5.1 in Table 3) has particularly large errors, all $^{207}\text{Pb}^*/^{206}\text{Pb}^*$ ratios agree to within analytical precision, yielding a mean of 0.069841 ± 0.000399 (MSWD = 0.3), equivalent to an age of 923.7 ± 11.8 Ma (1σ). Corresponding $^{206}\text{Pb}^*/^{238}\text{U}$ ratios, however, are dispersed beyond analytical precision, yielding ages between 900 and 972 Ma, with analysis 5.1 (not shown in Fig. 7a), at 726 Ma, having clearly undergone loss of radiogenic Pb. A two-error regression through all data yields a discordia with intercepts at 924 ± 20 and -3 ± 427 Ma (both 1σ), which does not indicate any ancient loss of radiogenic Pb. On this basis, the mean $^{207}\text{Pb}^*/^{206}\text{Pb}^*$ age of 924 ± 25 Ma (95% confidence limits) is taken as the best estimate of the age of the Mativa zircons.

Twenty-six analyses were conducted of 26 zircons from Bata Kimenga granite sample #1027. Uranium concentrations range from 90 to 660 ppm, with a mean of 270 ppm; Th/U ratios range from 0.4 to 0.8, and average 0.6. Values for f_{206} are less than 0.1% for 21 analyses, and range between 0.1 and 0.3% for the remaining six analyses. As with sample RG117.805, the $^{207}\text{Pb}^*/^{206}\text{Pb}^*$ ratios agree to within error, but the $^{206}\text{Pb}^*/^{238}\text{U}$ results are dispersed beyond analytical uncertainty, the latter ratios yielding ages between 822 and 980 Ma (Fig. 7b). The mean $^{207}\text{Pb}^*/^{206}\text{Pb}^*$ ratio is 0.069620 ± 0.000231 (MSWD = 0.2), equivalent to an age of 917.2 ± 6.8 Ma (1σ). Regression of all data yields concordia intercepts of 917 ± 7 and -21 ± 243 Ma (both 1σ). These zircons appear to have undergone variable amounts of mainly recent Pb loss, hence the best estimate of the age of the Bata Kimenga zircons is given by the mean $^{207}\text{Pb}^*/^{206}\text{Pb}^*$ age of 917 ± 14 Ma (95% confidence limits).

4.4. Discussion of SHRIMP geochronology

Previous multigrain isotope dilution analyses of zircons from two samples of Noqui granite (RG71.299, RG13.122; total of five fractions), yielded compositions within error of concordia, but indicated ages from 950 to 650 Ma (Delhal et al., 1971; Cahen et al., 1976). A regression through four analyses prompted Cahen et al. (1976) to suggest that the Noqui granite crystallised at ca. 750 Ma, and that their one significantly older fraction contained xenocrystic zircons. Cahen et al. (1976) also noted the possibility, however, that the zircons crystallised at about 1000 Ma and had undergone variable amounts of Pb loss. The microscale sampling ability of the ion microprobe permitted the least altered and least damaged areas of the zircons to be analysed. The results indicate an age of crystallisation of 999 ± 7 Ma, validating the second interpretation of Cahen et al. (1976).

The mean $^{206}\text{Pb}^*/^{238}\text{U}$ ages for the two Mayumbian rhyolite samples (911.9 ± 2.5 , 920.3 ± 3.2 Ma, both $\pm 1\sigma$) are distinguishable statistically, and the younger age for sample #1984 is in accordance with observed field relations. The dif-

Table 3
 Ion microprobe U–Pb zircon data for Mayumbian granite samples RG117.805 and # 1027

Grain area	²³⁸ U (ppm)	Th/U	<i>f</i> ₂₀₆ (%)	²⁰⁷ Pb*/ ²⁰⁶ Pb*		²⁰⁶ Pb*/ ²³⁸ U		²⁰⁶ Pb*/ ²³⁸ U Age	
					(± 1σ)		(± 1σ)	(Ma)	(± 1σ)
<i>Sample RG117.805</i>									
1.1	243	0.67	0.017	0.07078	0.00120	0.15012	0.00235	951.1	34.4
2.1	80	0.61	0.016	0.07011	0.00147	0.15899	0.00436	931.6	42.5
3.1	181	0.34	0.125	0.06804	0.00280	0.16205	0.00354	869.9	83.0
4.1	121	0.77	0.023	0.06991	0.00253	0.15894	0.00262	925.7	72.6
5.1	148	0.65	0.477	0.06675	0.00469	0.11929	0.00769	830.0	140
6.1	121	0.93	0.016	0.06971	0.00129	0.15722	0.00383	919.7	37.7
7.1	196	0.57	0.040	0.07030	0.00123	0.16273	0.00263	937.2	35.4
8.1	138	0.68	0.103	0.07103	0.00199	0.16153	0.00282	958.4	56.1
9.1	103	0.69	0.261	0.07022	0.00256	0.15787	0.00318	934.8	72.9
10.1	87	0.66	0.016	0.07034	0.00121	0.15633	0.00285	938.4	34.9
11.1	118	0.70	0.017	0.07027	0.00278	0.15650	0.00451	936.3	79.1
12.1	161	0.92	0.083	0.06938	0.00143	0.14954	0.00262	910.2	41.8
13.1	138	0.78	0.132	0.07020	0.00255	0.15442	0.00249	934.1	72.7
14.1	230	0.31	0.044	0.07109	0.00229	0.15607	0.00230	960.1	64.6
15.1	177	0.71	0.017	0.06945	0.00108	0.16230	0.00252	912.2	31.6
16.1	138	0.73	0.120	0.06839	0.00322	0.15080	0.00209	880.4	94.5
17.1	115	0.65	0.017	0.06791	0.00139	0.16211	0.00375	865.9	42.0
<i>Sample # 1027</i>									
1.1	156	0.51	0.015	0.06946	0.00205	0.15895	0.00242	912.5	59.7
2.1	498	0.81	0.006	0.06901	0.00092	0.15465	0.00161	899.2	27.2
3.1	663	0.42	0.017	0.06986	0.00067	0.15701	0.00216	924.1	19.6
4.1	284	0.68	0.017	0.06964	0.00078	0.15502	0.00223	917.9	22.9
5.1	385	0.72	0.023	0.06877	0.00116	0.14915	0.00181	891.8	34.4
6.1	347	0.65	0.026	0.06964	0.00140	0.15347	0.00195	917.7	40.8
7.1	445	0.60	0.017	0.07055	0.00110	0.14776	0.00182	944.5	31.6
8.1	216	0.57	0.079	0.06982	0.00134	0.15992	0.00234	923.2	39.0
9.1	133	0.56	0.017	0.07006	0.00099	0.15985	0.00264	930.2	28.7
10.1	210	0.59	0.017	0.07007	0.00084	0.15703	0.00202	930.5	24.3
11.1	345	0.75	0.046	0.06880	0.00117	0.15689	0.00166	892.6	34.7
12.1	456	0.66	0.111	0.06943	0.00108	0.14761	0.00125	911.6	31.7
13.1	254	0.59	0.067	0.06939	0.00192	0.14820	0.00260	910.3	56.0
14.1	94	0.73	0.022	0.07078	0.00259	0.16412	0.00502	951.1	73.0
15.1	230	0.70	0.066	0.06878	0.00153	0.16122	0.00285	892.0	45.4
16.1	516	0.81	0.082	0.06968	0.00106	0.13616	0.00169	918.9	31.1
17.1	91	0.54	0.142	0.06878	0.00336	0.14517	0.00350	892.2	97.8
18.1	145	0.64	0.137	0.07026	0.00243	0.15459	0.00250	935.8	69.5
19.1	145	0.56	0.054	0.06908	0.00216	0.15959	0.00307	901.2	63.2
20.1	220	0.62	0.054	0.06949	0.00125	0.15194	0.00163	913.3	36.5
21.1	207	0.55	0.017	0.07027	0.00088	0.14692	0.00261	936.2	25.6
22.1	173	0.79	0.304	0.06981	0.00415	0.15441	0.00699	922.8	118
23.1	211	0.58	0.282	0.06827	0.00290	0.15568	0.00272	876.8	85.5
24.1	174	0.71	0.077	0.06937	0.00238	0.14097	0.00266	909.8	69.0
25.1	255	0.65	0.017	0.06975	0.00086	0.15211	0.00269	921.0	25.0
26.1	258	0.62	0.178	0.06871	0.00103	0.15221	0.00164	890.0	30.8

*f*₂₀₆ is the proportion of common ²⁰⁶Pb in measured ²⁰⁶Pb, estimated using ²⁰⁴Pb. Pb* indicates radiogenic Pb.

Table 4
Major and trace element compositions of six Gangila basalts and Mayumbian felsic rocks in Bas-Congo

Sample	Gangila basalts						Mayumbian felsic rocks					
							Granites			Rhyolites		
	432	417	2478	431	1315	2485	866	908	1027	2336	2315	1981
SiO ₂	46.93	47.68	50.16	51.00	47.67	50.99	73.95	66.45	76.85	71.47	68.22	73.01
TiO ₂	1.09	0.70	0.81	0.85	0.87	0.94	0.33	1.11	0.15	0.57	0.64	0.47
Al ₂ O ₃	14.88	13.98	7.24	14.14	15.77	20.36	13.21	13.68	11.83	12.20	11.22	13.04
Fe ₂ O ₃	2.28	5.96	6.11	3.31	5.89	3.57	1.74	0.56	0.59	0.23	1.93	1.48
FeO	8.29	4.83	10.58	5.97	5.11	3.75	1.26	5.30	1.66	3.38	5.66	1.68
MnO	0.16	0.18	0.16	0.17	0.17	0.11	0.02	0.08	0.02	0.17	0.15	0.07
MgO	9.24	7.22	6.98	6.82	5.36	2.80	0.43	1.43	0.11	0.28	0.46	0.54
CaO	10.27	14.41	13.46	12.09	15.79	9.07	1.15	3.31	0.53	1.04	1.18	0.67
Na ₂ O	1.85	0.71	1.50	2.13	0.31	4.44	2.82	2.48	2.77	2.75	1.52	3.37
K ₂ O	0.13	0.15	0.13	0.12	0.07	0.68	4.85	3.81	5.15	5.45	5.79	5.43
P ₂ O ₅	0.19	0.12	0.12	0.13	0.16	0.27	0.07	0.31	0.02	0.10	0.21	0.06
L.O.I.	3.93	3.70	2.43	2.23	2.83	2.52	0.58	1.00	0.42	1.42	1.55	0.42
Total	99.24	99.64	99.68	98.96	100.00	99.5	100.41	99.52	100.1	99.06	98.53	100.24
Rb	3	4	4	3	2	28	252	166	433	188	223	268
Sr	269	108	209	196	294	305	98	222	22	13	55	41
Y	23	16	17	15	17	29	65	55	92	84	107	205
Zr	124	53	84	82	88	156	177	355	197	780	356	486
Ba		74		215			696	1268	90	254	1071	907
V		248	246	234	269		20	76	6	13	24	14
Sc	39	37	38	37	34	18	5	15	3	4	12	6
Cr	258	651	247	271	128	40	61	52	68	35	119	59
Co	60	49	51	44	40	27	4	12	2	1	12	6
La	14.2	4.46	7.46	7.10	5.63	26.9	87.7	66.3	85.1	125	108	146
Ce	28.3	10.1	16.4	16.3	11.7	52.0	180	140	174	241	180	233
Nd	14.9	6.07	10.3	9.01	8.12	23.1	69.5	62.4	60.6	97	88	105
Sm	3.06	1.57	2.11	2.11	1.92	3.94	11.3	10.6	10.3	15.3	14.1	16.7
Eu	1.10	0.68	0.91	0.82	0.87	1.24	1.28	1.97	0.28	2.89	2.31	2.36
Tb	0.58	0.36	0.43	0.46	0.42	0.65	1.43	1.24	1.27	1.80	1.79	2.54
Dy		2.51	2.58	2.26	2.36		8.12	6.78	9.74	10.5	9.8	16
Ho	0.75					0.83						
Yb	1.92	1.64	1.62	1.67	1.55	2.35	5.09	4.08	7.01	6.05	6.02	9.53
Lu	0.32	0.37	0.28	0.43	0.34	0.37	0.75	0.61	1.06	0.95	0.91	1.55
Hf	2.06	0.96	1.37	1.32	1.05	3.09	5.94	10.2	7.29	17.20	9.05	12.4
Ta	0.75	0.14	0.20	0.22	0.27	0.50	1.43	1.67	2.69	2.28	1.31	2.81
Th	1.23	0.37	0.75	0.65	0.46	4.57	37	21	81	28	22	40
U	0.42	0.17	0.15	0.26	0.15	0.86	5.98	4.05	18	3.75	3.87	8.28

Selected from 84 previous analyses of major elements+Y and Zr in Tack (1975a,b, 1979a) and 26 analyses of other trace elements in Namegabe (1981); Rb, Sr, Sm, and Nd analysed by ICP-MS (Appendix A.2.).

ference in age between the two samples, and hence an estimate of the duration of felsic magmatism, is 8 ± 4 Ma (1σ) between about 920 and 912 Ma. Although less precisely determined, the ages ($\pm 1\sigma$) of the two Mayumbian granites (923.7 ± 11.8 Ma for the Mativa granite; 917.2 ± 6.8 Ma for the Bata Kimenga granite; both in accordance with observed field relations) are not significantly different from each other, nor from those determined for the Mayumbian rhyolites. The data are thus consistent with the granites and rhyolites being essentially coeval at about 918 ± 10 Ma. Cahen et al. (1978) combined multigrain zircon analyses from five different Mayumbian granite and rhyolite samples to derive a concordia intercept age of 1027 ± 56 Ma. Based on comparison with results presented here, however, the multigrain fractions employed by Cahen et al. (1978) would appear to have undergone variable amounts of Pb loss and to have contained some xenocrystic zircons. Indeed, two xenocrystic zircons analysed from sample # 58 provide evidence that the Mayumbian igneous suite was emplaced through 'Kimezian' basement of Palaeoproterozoic age.

5. Geochemistry and Nd–Sr isotopes: the Gangila and Mayumbian sequences as a continental flood basalt province

Previous studies considered the Gangila mafic series to be continental tholeiitic within-plate basalts (Tack, 1975b), modern island arc tholeiites (Namegabe, 1981), or E-MORB, possibly linked to a back-arc environment (Franssen and André, 1988). The Mayumbian volcanic–plutonic sequence, considered as a single cogenetic series (Tack, 1975a, 1979a; Namegabe, 1981) has been suggested to result from partial melting of crustal rocks (Franssen and André, 1988).

New trace element and Sr–Nd isotopic analyses of available samples (Tables 4 and 5) have been performed in an attempt to clarify the palaeo-environment. Major element compositions of the same samples have been published previously (Tack, 1975a,b, 1979a). Although based on few samples, the signatures of both the Gangila and Mayumbian sequences are sufficiently similar to those of conti-

ental flood basalts (CFBs) and associated felsic magmatism to propose such an origin.

Most Gangila basalts display intermediate values of 9–5% (uppermost sample 2485 at 2.8%) for MgO, and $Mg \# [100 MgO/(MgO + FeO_t)]$ varies from 43 to 29. They also are low in K_2O ($< 0.2\%$; sample # 2485 at 0.68%). REE patterns of Gangila basalts (Fig. 8a) display LREE enrichment with a small Eu positive anomaly suggesting some cumulate plagioclase. Samples # 432, # 2478, # 431 and # 1315 indicate that REE contents decrease together with MgO (from 9.2 to 5.4% MgO, ΣREE decreases from 64 to 31 ppm). If this effect is caused by differentiation, it requires a partition coefficient for pyroxene and/or amphibole above unity. Another possibility is to mix a basaltic liquid with a more felsic REE-poor contaminant. There are insufficient samples available to discriminate between these options, although the first possibility seems easier to apply. In contrast, the uppermost basalt (# 2485) is comparatively enriched in REE. Its LREE enrichment is also higher ($La_N/Yb_N = 7.7$ vs. 5–2.4 for main basalt group).

The Mayumbian felsic rocks (66–76% SiO_2) are rich in K_2O (up to 5.8%) and rather low in Na_2O (1.5–3.4%). Variation in Al_2O_3 (11.2–13.7%) explains the variability of the agpaite index ($Na_2O + K_2O/Al_2O_3$, in molar proportion) from 0.64 to 0.93. REE content is high (300–500 ppm) as are the Th and U contents (21–81 and 4–18 ppm, respectively). These geochemical characteristics point to a potassic series.

REE patterns in the Mayumbian felsic rocks (Fig. 8b) show strong enrichment in LREE (180–400 \times chondritic for La) but also in HREE (16–38 \times chondritic for Yb). La_N/Yb_N ratios vary from 8 to 14 (7.7 for the Gangila upper basalt). Concentrations of REE are higher in rhyolites than in granites but the shape of REE patterns are similar. Except for Eu, the Gangila upper basalt possesses a parallel REE pattern. It would thus be easy to generate the Mayumbian felsic rocks by differentiation from such a basalt which, moreover, has a similar ϵ_{Nd} (Table 5).

Spidergrams normalised to MORB for the Gangila basalts (Fig. 9a) (sample # 417 with high Cr has been removed for clarity) show that a negative anomaly such as that of Hf is a consequence of differentiation (or mixing), rather than

Table 5
Sr and Nd isotopic data for Gangila and Mayumbian magmatic rocks

Sample	Rb (ppm)	Sr (ppm)	$^{87}\text{Rb}/^{86}\text{Sr}$	$^{87}\text{Sr}/^{86}\text{Sr}$	2σ (10^{-6})	Sr_i (925 Ma)	Sm (ppm)	Nd (ppm)	$^{147}\text{Sm}/^{144}\text{Nd}$	$^{143}\text{Nd}/^{144}\text{Nd}$	2σ (10^{-6})	ϵ_{Nd} (925 Ma)	T_{DM}
<i>Gangila (Upper Zadinian)</i>													
1315	2	294	0.01968	0.705285	8	0.705025	1.92	8.12	0.1430	0.512285	11	−0.53	1628
432	3	269	0.03229	0.711572	9	0.711145	3.06	14.9	0.1242	0.512018	9	−3.52	1741
431	3	196	0.04428	0.705009	14	0.704423	3.94	23.1	0.1031	0.511990	15	−1.57	1449
430	3	175	0.04959	0.704928	13	0.704272							
2478	4	209	0.05537	0.705046	8	0.704314	2.11	10.3	0.1239	0.511996	10	−3.91	1773
417	4	108	0.1072	0.706327	10	0.704911	1.57	6.07	0.1564	0.512257	10	−2.67	2090
2485	28	305	0.2658	0.712063	9	0.708549	3.94	23.1	0.1031	0.511440	7	−12.32	2213
<i>Mayumbian</i>													
866	252	98	7.51	0.803320	10	0.704008	11.3	69.5	0.09831	0.511428	13	−11.99	2135
908	166	222	2.170	0.736213	15	0.707523	10.6	62.4	0.1027	0.511543	8	−10.26	2060
1027	433	22	60.75	1.383608	11	0.580369	10.3	60.6	0.1028	0.511492	8	−11.26	2133
1981	268	41	19.29	0.909860	9	0.654779	16.7	105	0.09617	0.511491	10	−10.50	2013
2315	223	55	11.87	0.827190	11	0.670232	14.1	88	0.09689	0.511650	11	−7.48	1815
2336	188	13	44.10	1.252230	13	0.669206	15.3	97	0.09537	0.511263	8	−14.86	2298

T_{DM} model ages have been calculated following Nelson and De Paolo (1985).

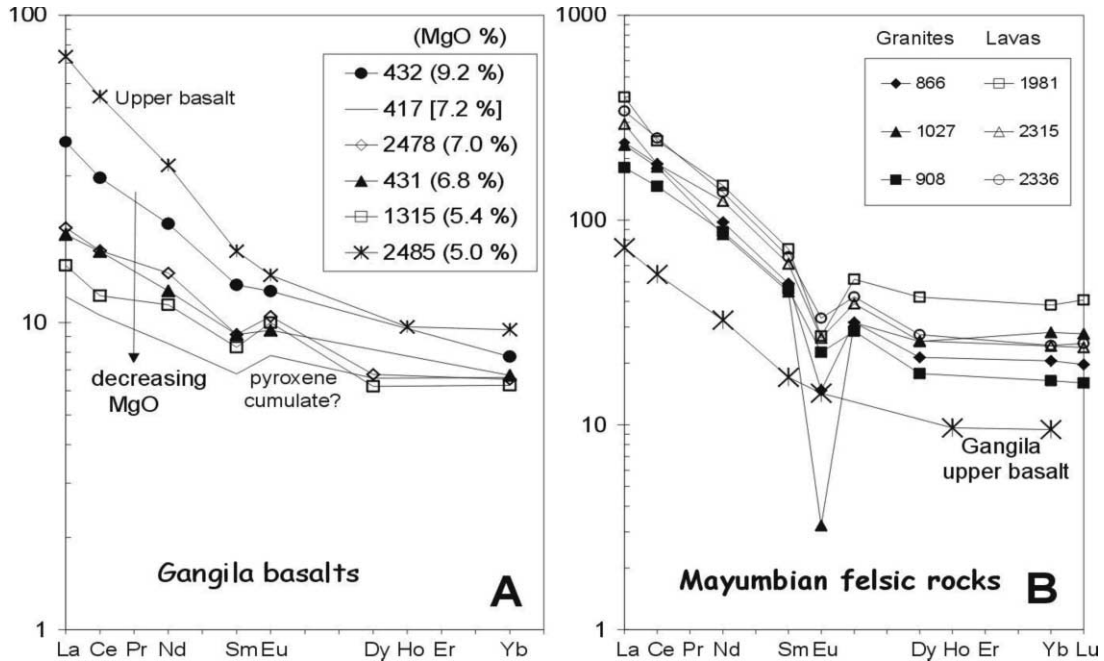


Fig. 8. Rare earth elements normalised to chondrites (Taylor and McLennan, 1985) for (a) the Gangila basalts (upper Zadinian) and (b) Mayumbian felsic magmatic rocks.

a characteristic of the source. Discrimination diagrams using Hf could therefore yield invalid results. In general, the most mafic sample (#432) has the highest concentrations, and thus represents a minimum estimate for the composition of the original magma. This #432 basalt pattern is parallel to a mean of different CFB provinces (Thompson et al., 1983). A mean of the Wollaston and Hold with Hope lower basaltic series (East Greenland; Thirlwall et al., 1994) displays a similar low pattern.

Spidergrams normalised to MORB for the felsic Mayumbian rocks (Fig. 9b) are very similar to the Paraná rhyolites, in particular to the low-Ti equigranular, nearly aphyric, Santa Maria series (Garland et al., 1995), whose mean spidergram follows closely that of the Mayumbian. Both series have similar SiO₂ contents (mean of 70.6% for Santa Maria and of 71.7% for the Mayumbian). Spidergrams of the Mayumbian felsic rocks are also similar in shape to the Gangila upper basalt except for the late effects on Ba, P and Ti of feldspar, apatite and Fe–Ti oxide fractionation,

respectively. Other characteristics preserved include a weakly negative Ta anomaly or a slightly positive Zr anomaly. Except for Ba, P and Ti, the reported trace elements behaved throughout the Mayumbian felsic rocks as incompatible elements (Table 4), and the Gangila upper basalt could fit the characteristics of the parent magma. In contrast, the Gangila main basaltic series does not fit a possible parent magma for the upper basalt.

Sr isotopes do not provide reliable initial values due to disturbance: the six Mayumbian felsic samples yield an errorchron (808 ± 98 Ma, 0.705 ± 0.042 , MSWD = 26) that changes insignificantly if the upper basalt is taken into account (807 ± 75 Ma, 0.706 ± 0.029 , MSWD = 25). These 'ages' do not correspond directly to geological events. They probably lie between the emplacement age of the Mayumbian felsic sequence (ca. 920–910 Ma; see Section 4.4) and the age of the isotopic disturbance, maybe of Pan-African age (ca. 566 Ma; see Section 1). Owing to this perturbation, Sr isotopic initial ratios (Sr_i) range at 920 Ma between 0.707 and values below 0.7 (Table 5) and render useless

the classical Sr_i versus ϵ_{Nd} diagram. Lower Rb/Sr ratios in the basalts allow the calculation of more reliable Sr_i that range at 920 Ma from 0.7043 to 0.7050 except sample # 432 (0.7111) and the upper basalt (0.7085).

Gangila basalts have ϵ_{Nd} at 920 Ma varying from -3.9 to -0.5 (mean $\epsilon_{Nd} = -2.4 \pm 1.2$; Fig. 10a) except the upper basalt that has a much lower ϵ_{Nd} (-12.3) within the range of the Mayumbian felsic rocks ($\epsilon_{Nd} = -11 \pm 2$; Fig. 10a). T_{DM} model ages (Fig. 10b) in the Gangila basalts vary from

1450 to 1770 Ma (plus sample # 417 at 2090 Ma) with a mean of 1736 ± 105 Ma (1648 ± 146 Ma without sample # 417). In the Mayumbian felsic rocks, T_{DM} model ages vary from 1818 to 2298 Ma with a mean of 2076 ± 65 Ma. The T_{DM} model age of the upper basalt (2213 Ma) lies within the Mayumbian range. This suggests that the higher Sr_i value of sample # 432 is due to a later disturbance not affecting the Nd isotopes while the upper basalt # 2485 characteristics are pristine, its Nd and Sr isotopes being correlated.

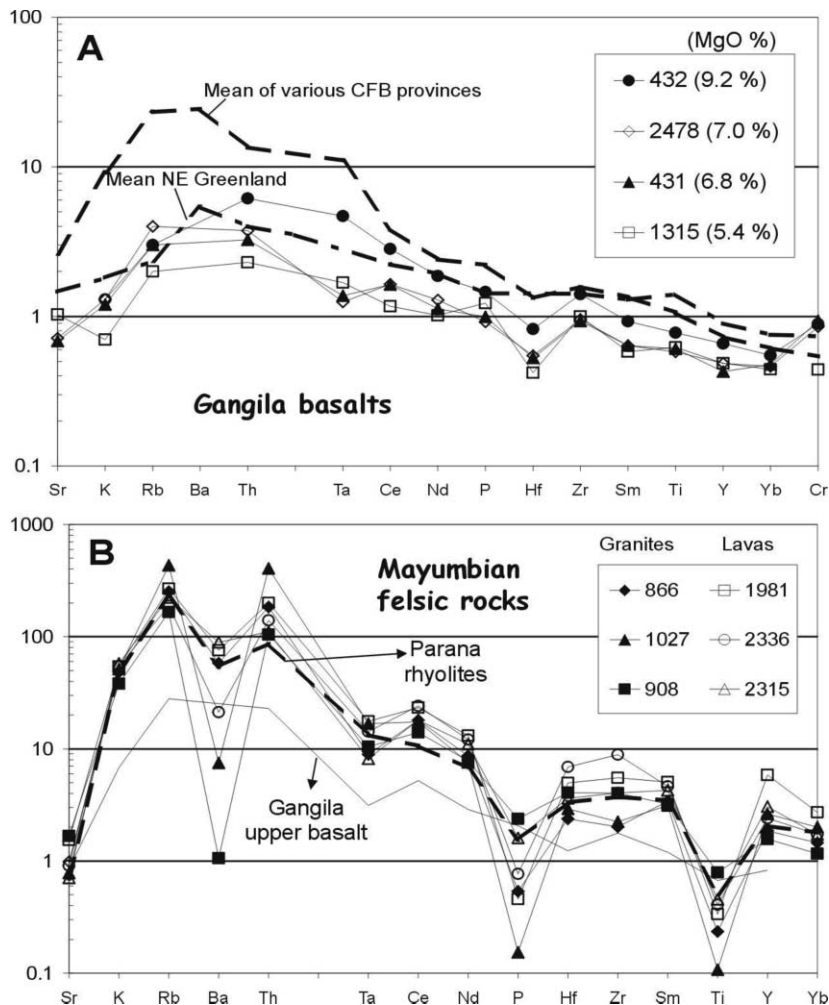


Fig. 9. Spidergrams normalised to MORB (Pearce, 1983) for (a) the Gangila basalts (upper Zadinian) and (b) Mayumbian felsic magmatic rocks. Mean NE Greenland CFB from Thirlwall et al. (1994), mean of various CFB provinces from Thompson et al. (1983); Paraná rhyolites (mean of Santa Maria series) from Garland et al. (1995).

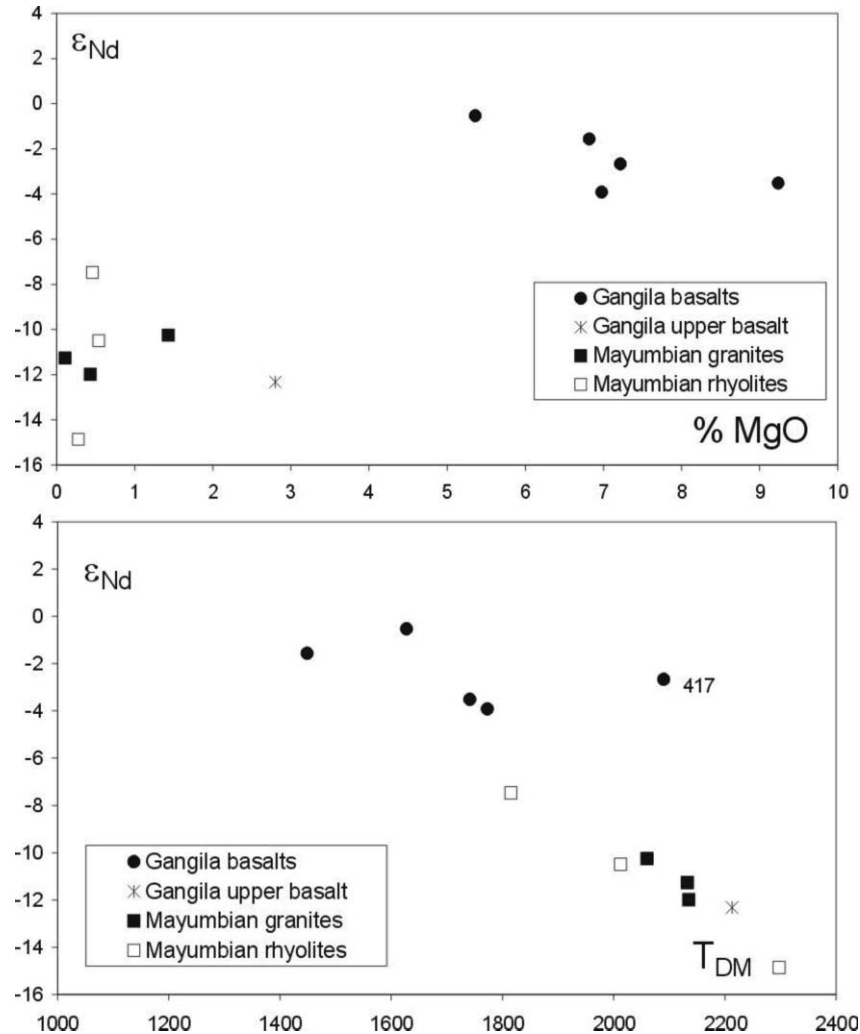


Fig. 10. (a) Percent MgO vs. ϵ_{Nd} at 925 Ma (mean of ca. 920 and 930 Ma); (b) T_{DM} model ages (using parameters of Nelson and De Paolo, 1985) vs. ϵ_{Nd} at 925 Ma.

It thus appears that the geochemical break is located in the upper part of the Gangila basaltic series and not at the classical lithostratigraphic break between Zadinian and Mayumbian Groups (Fig. 4).

6. Relationships between Gangila and Mayumbian magmatism

The Gangila basalts are unlikely to be the source of the upper Gangila basaltic series that

appears surprisingly closer to the Mayumbian rhyolites. Trace element patterns of the Gangila basalts are similar to those of CFBs, in particular those at the base of the volcanic pile, in agreement with their mean ϵ_{Nd} at -2.4 ± 1.2 , a value not far from bulk earth, and typical of CFBs. Mayumbian granites and rhyolites are enriched in many elements and display chemical compositions intermediate between potassic and alkaline series. The Gangila upper basalt could represent the parent magma, a hypothesis that has to be tested further. Mayumbian felsic rocks and the Gangila upper

basalt share similar ϵ_{Nd} (-11 ± 2 and -12.3 , respectively) and T_{DM} values (1818–2298 and 2213 Ma). These characteristics imply an old source, which could be enriched lithospheric mantle or crust. If the upper basalt (51% SiO_2) does correspond to the parent magma, an old (Kimezian? Archaean?) enriched lithospheric mantle or mafic lower crust would be favoured (Turner and Hawkesworth, 1995; Kirstein et al., 2000).

Felsic volcanics associated with CFBs are known in the Deccan and Paraná provinces, where they also overlie the basalts (Lightfoot et al., 1987; Garland et al., 1995). Geochemical and isotopic studies have suggested that, in the Deccan province, the felsic rocks originated from partial melting of a CFB equivalent at depth (Lightfoot et al., 1987). In Paraná, high-Ti rhyolites were considered to have formed from a liquid line of descent from the CFB magma, accompanied by some crustal contamination during differentiation and low-Ti rhyolites from the melting of a CFB equivalent at depth (Garland et al., 1995). In all cases, partial melting of felsic crust is precluded. When the ultimate source is considered, the two origins are not significantly different, because the CFB source is considered to be the lithospheric mantle. In Bas-Congo, a liquid line of descent from the main basalt series to explain the felsic magmatism is not applicable. By comparison with Paraná, partial melting of CFB equivalent at depth (i.e. mafic lower crust; Kirstein et al., 2000), coupled with subsequent crystal fractionation or melting of the enriched lithospheric mantle itself could be adopted for Mayumbian felsic rocks. This suggests that the Gangila mafic rocks are not much older than the Mayumbian, i.e. in the range 930–920 Ma.

7. Model of early Neoproterozoic evolution and magmatism in the framework of Rodinia breakup: initial transtensional rifting prior to breakup

The limited effects of the Pan-African orogeny in the median and external domains of the West Congo belt can be attributed to the passive margin conditions that prevailed during part of the

Neoproterozoic in this area [lower West Congolian Group resting directly on the Archaean craton (Fig. 2) with no subduction below this area during the Neoproterozoic] and to the thick lithospheric mantle which imparted high rigidity to the Congo craton during the Pan-African orogeny (Black and Liégeois, 1993). This also explains the polarity in deformation and metamorphic grade from west to east, the absence of Pan-African magmatism and the excellent preservation of early Neoproterozoic rocks. In the central, flexured segment of the West Congo belt, abundant magmatism was concentrated in early Neoproterozoic times, characterised by peralkaline granites and rhyolites followed by voluminous mafic and felsic lavas (ca. 5000–6000 m), the latter in association with K-rich granites.

A model of transtension of the lithosphere followed by transpression has been proposed to explain the Neoproterozoic evolution of a segment of the Pan-African belt along the Atlantic coast, close to the Namibia–South Africa border (Gariép and Vanrhijnsdorp belts; Gresse, 1995). This model can be extended to the north into the West Congo belt (Fig. 11).

Following a period of stability during the Mesoproterozoic, geochemical evolution of the West Congo belt can be linked to early Neoproterozoic (ca. 1000–910 Ma) dextral transtension. This process would have induced incipient rifting, early Zadinian sedimentation and small amounts of peralkaline melt along a transverse mega-shear system in a pre-Pan-African (Kimezian) basement uplift zone (Noqui and Palabala; ca. 1000 Ma; Fig. 11a and Fig. 12a). Subsequently, lithospheric extension in pull-apart rifts along the Congo cratonic boundary triggered extensive continental magmatism (Anderson, 1994, 1995; Molina and Ussami, 1999). Increased asthenospheric upwelling induced major rifting accompanied by higher degrees of partial melting of the lithospheric mantle (Gangila CFBs; ca. 930–920 Ma; Fig. 11b and Fig. 12b). Finally, melts derived from colder and older K-enriched lithospheric mantle (Turner and Hawkesworth, 1995) gave rise to the Mayumbian felsic magmatism (ca. 920–910 Ma; Fig. 11c and Fig. 12c; Luttinen and Furnes, 2000). This sequence of events implies

that the melting region became shallower with time. Note that the Zadinian and Mayumbian magmatic events thus have no link with Neoproterozoic subduction.

Taking into account recent constraints from the Araçuaí belt in Brazil (Pedrosa-Soares et al., 2001) that indicate an oceanic stage at ca. 800 Ma (ophiolitic remnants), we suggest that a breakup event occurred between ca. 910 and 800 Ma. As the ophiolite is probably a late event, breakup is likely to have begun not long after Zadinian–Mayumbian rifting. The latter did not correspond to an aborted rift but was the initial stage of breakup in this part of the Rodinia supercontinent.

By the end of the Neoproterozoic (ca. 566 Ma), the Pan-African Brasiliano-Araçuaí belt, adjacent to the São Francisco craton of Brazil, had collided to the east with the passive margin of the Congo craton inducing relatively limited effects on the West Congo belt. This occurred during the

assembly of Gondwanaland.

Our new U–Pb SHRIMP zircon ages, coupled with field observations, are similar to observations of the Deccan traps (Sheth, 1999); early manifestations include local extension along a major lithospheric discontinuity, rift-type sedimentation (cf. lower Zadinian) and peralkaline felsic magmatism (cf. Noqui and Palabala at ca. 1000 Ma). Mafic and felsic continental flood volcanism occurred about 70 Ma later (cf. Gangila and Mayumbian). The latter constitutes the climax of continental rifting prior to the rift-drift transition and thus not its initiation.

As for the Deccan province (Sheth, 1999), a mantle plume model is inadequate in Bas-Congo, the CFB volcanism does not follow a doming of the crust and does not constitute the first magmatic event in the area, as would be expected according to the mantle plume hypothesis (Campbell and Griffiths, 1990; Hill et al., 1992; Anderson, 1995).

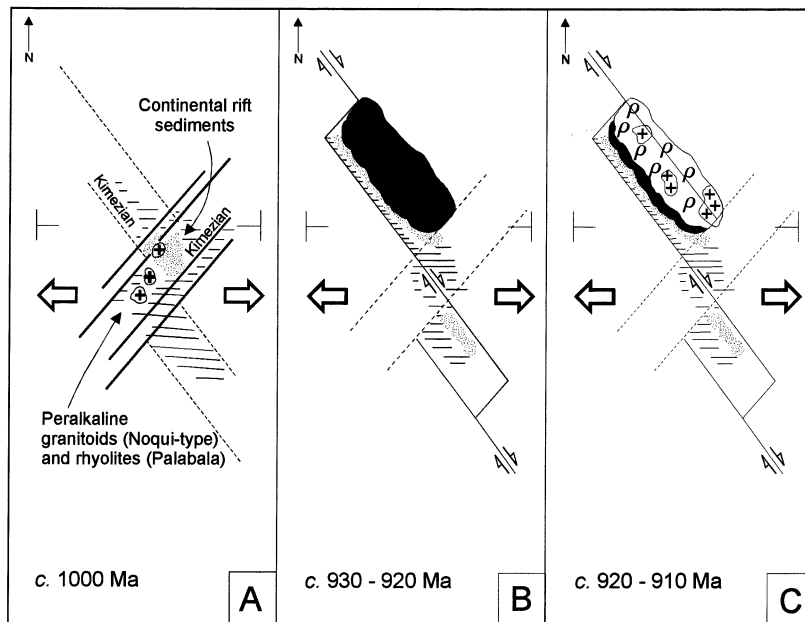


Fig. 11. Model of dextral transensional rifting and associated magmatic events along the western edge of the Congo craton prior to Rodinia breakup. (a) ca. 1000 Ma, transverse mega-shear setting in Kimezian basement uplift zone, initial continental rifting and peralkaline magmatism; (b) ca. 930–920 Ma, major rifting associated with pull-apart rifts and emplacement of Gangila CFBs; (c) ca. 920–910 Ma, major rifting continues, with emplacement of Mayumbian felsic volcanic–plutonic magmatism. Symbols; strips, Palaeoproterozoic Kimezian Supergroup; dots, Zadinian rift sediments; full black, Gangila CFBs; ρ , Mayumbian rhyolites, +, Mayumbian granites; \perp , localisation of the cross-sections of Fig. 12.

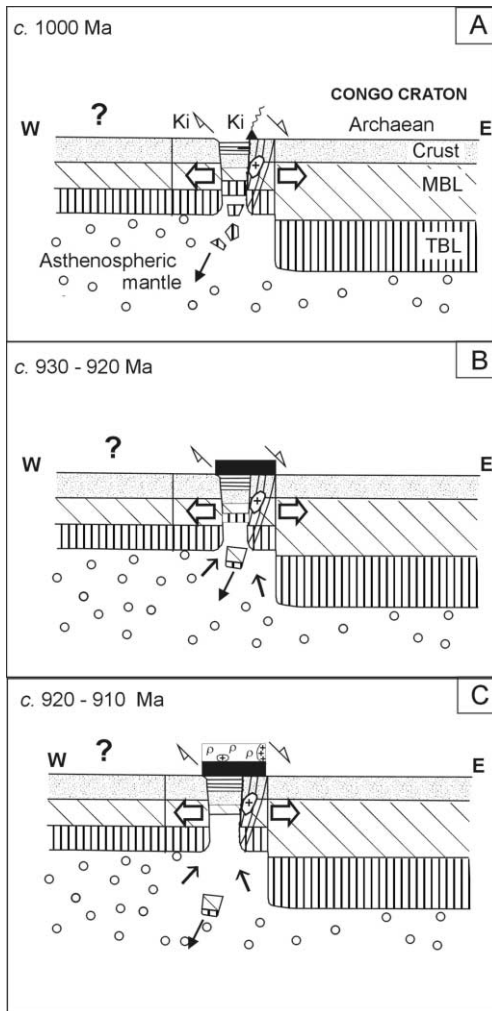


Fig. 12. E–W cross-sections (not to scale) of dextral transtension rifting model and associated magmatic events along the western edge of the Congo craton (locations shown on plan view in Fig. 11); (a–c), same as in Fig. 11; MBL, mechanical boundary layer; TBL, thermal boundary layer (Black and Liégeois, 1993); transtensional rifting developed preferentially in the thinner Palaeoproterozoic lithosphere at the contact with the thicker lithosphere of the Archaean craton (Durrheim and Mooney, 1991); Ki, ca. 2.1 Ga Palaeoproterozoic basement (Kimezian Supergroup); ?, according to our data, anticipated prolongation to the west of the Kimezian (Ki) basement into an unknown continent; however, taking into account the data in Brazil of Pedrosa-Soares et al. (2001), this might well be the Palaeoproterozoic Transamazonian belt (Brazilian equivalent of the Kimezian), followed to the west by the Archaean São Francisco craton.

8. Conclusions

Revision of geological data on the West Congo Pan-African belt has led to the compilation of an updated geological map of the entire belt and the elaboration of a synthetic type cross-section and revised lithostratigraphic column, in particular for the 'West Congo Supergroup'. New SHRIMP U–Pb age measurements constrain the Zadinian and overlying Mayumbian Groups as major, early Neoproterozoic, magmatic events between ca. 1000 and 910 Ma, marking at the western edge of the Congo craton the rifting of Rodinia before its breakup. Subsequently, during the Neoproterozoic, Bas-Congo behaved as a passive margin of the Congo craton, characterised by deposition of about 4000 m of platform sediments (lower part of West Congolian Group). At the end of the Neoproterozoic, due to its passive margin character and to the presence of the thick lithosphere of the adjacent Congo craton, Bas-Congo was involved only to a limited extent in the Pan-African orogeny (end at ca. 566 Ma).

The Noqui peralkaline granite, considered previously to post-date the Pan-African orogeny in the West Congo belt, has yielded a U–Pb SHRIMP age of ca. 1000 Ma. This age marks the onset of early transtension along the western edge of the Congo craton, characterised at an initial stage by peralkaline magmatism (Noqui-type granites and Palabala rhyolites) and incipient rift sedimentation of the lower Zadinian Group.

The main magmatic events recorded in Bas-Congo are, however, voluminous CFBs (Gangila basalts, upper part of the Zadinian Group, between ca. 930 and 920 Ma) and extensive coeval felsic magmatic rocks (rhyolites and granites, Mayumbian Group) between ca. 920 and 910 Ma. U–Pb SHRIMP results indicate a short emplacement interval (8 ± 4 Ma; 1σ) for the 3000–4000 m thick felsic Mayumbian sequence.

Geochemically, the Zadinian and Mayumbian mafic–felsic magmatic association (ca. 6000 m thick) corresponds strongly to the Paraná or Decan CFB–rhyolite association. However, Mayumbian felsic rocks contain an older lithospheric component marked by lower ϵ_{Nd} than Gangila basalts (-12.3 vs. -2.4) and cannot be derived

simply from the latter (Luttinen and Furnes, 2000). The chronological succession of Noqui-type peralkaline granites and rhyolites, Gangila CFBs and Mayumbian felsic magmatism reflects an increase in the contribution of an old enriched lithosphere, suggesting that the magma source became shallower with time.

Finally, our results indicate that, unlike some other scenarios (e.g. Vellutini et al., 1983), there is no record of any geological sequence or geodynamic activity occurring at the western edge of the Congo craton during the Mesoproterozoic. This means that in the considered area, evidence for a local segment of Kibaran-aged or Grenville-aged belt is totally lacking. In contrast with previous interpretations (Lepersonne, 1974; Cahen et al., 1984; Boudzoumou and Trompette, 1988; Maurin, 1993; Trompette 1994; Unrug, 1996; Unrug et al., 1996; Hartzler, 1998), there is thus no 'Mayumbian' nor 'Zadinian' orogeny and also no aulacogen of Mesoproterozoic age, nor is there any evidence for the occurrence of Mesoproterozoic juvenile ophiolitic crust or a suture zone.

As such, this setting compares well with what is known at the northern edge of the Congo craton or in West Africa, where the cratonic blocks are Archaean or Palaeoproterozoic and the adjacent mobile belt segments are Pan-African, the latter marking Gondwanaland amalgamation at the end of the Neoproterozoic.

Acknowledgements

Zircon U–Pb analyses were conducted using the Western Australian SHRIMP facility, which is operated by a consortium consisting of Curtin University of Technology, the Geological Survey of Western Australia, and the University of Western Australia, with the support of the Australian Research Council (ARC). MW was supported by an ARC Postdoctoral Fellowship and the Tectonics Special Research Centre, which is supported by the ARC through its research centres program. The authors are very much indebted to A.B. Kampunzu, K.N. Sircombe, and C.McA. Powell for their careful and constructive reviews, allowing substantial improvement of an early draft.

This paper is a contribution to IGCP projects 418 ('Kibaran events in southern Africa') and 440 ('The assembly and breakup of Rodinia'). This is Tectonics Special Research Centre publication number 151.

Appendix A

A.1. Ion microprobe U–Pb zircon

Samples for U–Pb analysis were processed using standard density and magnetic techniques to concentrate the most dense and least magnetic fractions. A representative selection of zircon crystals was extracted from each concentrate by hand-picking under a binocular microscope. Zircons, together with chips of zircon standard, were cast in an epoxy mount, which was then polished to section the crystals for analysis. The mount was cleaned thoroughly, and the polished surface documented with transmitted and reflected light micrographs, then vacuum-coated with a ~500 nm layer of high-purity gold. To eliminate any residual water from the sampling surface, the mount was pumped down to high vacuum overnight in the SHRIMP sample lock prior to analysis.

Zircons were analysed using the SHRIMP II ion microprobe in Perth, Australia. U–Th–Pb ratios and absolute abundances were determined relative to the CZ3 standard zircon [$^{206}\text{Pb}^*/^{238}\text{U} = 0.91432$ (564 Ma); 550 ppm ^{238}U ; Pidgeon et al., 1994], using standard operating and data processing procedures similar to those described by Compston et al. (1984, 1992), Claoué-Long et al. (1995). Correction for common Pb in unknown zircons from each sample was made using measured ^{204}Pb . In most cases, corrections are sufficiently small to be insensitive to the choice of common Pb composition, and an average crustal common Pb composition (Cumming and Richards, 1975) appropriate to the age of each zircon was assumed.

Within a single analytical session, the relative $^{206}\text{Pb}^*/^{238}\text{U}$ ages of separate analyses are assessed correctly using their individual errors as calculated theoretically, or as observed empirically

within the analysis. Similarly, comparison of mean $^{206}\text{Pb}^*/^{238}\text{U}$ ages for samples analysed during the same analytical session are compared using errors computed from observed uncertainties. When the ‘absolute’ $^{206}\text{Pb}^*/^{238}\text{U}$ age is reported for the mean of a group, it is necessary to add, in quadrature, the uncertainty in the mean $^{206}\text{Pb}^*/^{238}\text{U}$ measured for the reference standard. Most results are quoted initially with 1σ uncertainties to facilitate statistical comparison; final uncertainties are reported at a 95% confidence level ($1\sigma \times \text{Student's } t$).

A.2. Sm–Nd and Rb–Sr

Following acid dissolution of the sample and Sr and Nd separation by ion-exchange resin, Sr isotopic compositions were measured on Ta simple filament and Nd isotopic compositions on triple Ta–Re–Ta filament, using a Micromass Sector 54 mass spectrometer. Repeated measurements of Sr and Nd standards show that between-run precision is better than 0.00002%. Within-run precision is higher. The NBS987 standard has given a value for $^{87}\text{Sr}/^{86}\text{Sr}$ of 0.710259 ± 0.000007 (normalised to $^{86}\text{Sr}/^{88}\text{Sr} = 0.1194$) and the MERCK Nd standard a value for $^{143}\text{Nd}/^{144}\text{Nd}$ of 0.512746 ± 0.000007 (normalised to $^{146}\text{Nd}/^{144}\text{Nd} = 0.7219$) during the course of this study. Decay constants used (Steiger and Jäger, 1977) are $1.42 \times 10^{-11} \text{ a}^{-1}$ (^{87}Rb) and $6.54 \times 10^{-12} \text{ a}^{-1}$ (^{147}Sm). Sr and Nd isotope ratios are listed in Table 5. Ages were calculated following Ludwig (1999).

A.3. Trace elements

Trace elements were analysed during the Ph.D. study of Namegabe (1981) by INAA at the Institute for Nuclear Sciences of the Gent University (Belgium), with a Thetis reactor and a Ge(Li) detector. Samples were prepared with wax (‘Hoechst Wachs Pulver’, 77% C; 13% H; 5% N; 5% O). Additional trace elements (Table 5) were analysed at RMCA according to the method described by Navez (1995), by ICP-MS (Fisons VG PlasmaQuad PQ2 Plus). Samples were prepared using lithium metaborate fusion.

References

- Alvarez, P., 1995. Les facteurs de contrôle de la sédimentation du Supergroupe Ouest-Congolien (Sud-Congo). Rampe carbonatée et activité biologique au Protérozoïque supérieur. Géologie régionale et générale. Documents du BRGM 239, p. 270, + annexes.
- Alvarez, P., Maurin, J.-C., 1991. Evolution sédimentaire et tectonique du bassin protérozoïque supérieur de Comba (Congo): stratigraphie séquentielle du Supergroupe Ouest-Congolien et modèle d’amortissement sur décrochements dans le contexte de la tectogénèse panafricaine. *Prec. Res.* 50, 137–171.
- Alvarez, P., Maurin, J.-C., Vicat, J.-P., 1995. La Formation de l’Inkisi (Supergroupe Ouest-congolien) en Afrique centrale (Congo et Bas-Zaïre): un delta d’âge Paléozoïque comblant un bassin en extension. *J. Afr. Earth Sci.* 20, 119–131.
- Anderson, D.L., 1994. The sublithospheric mantle as the source of continental flood basalts — the case against the continental lithosphere and plume. *Earth Planet Sci. Lett.* 123, 269–280.
- Anderson, D.L., 1995. Lithosphere, asthenosphere, and perisphere. *Rev. Geophys.* 33, 125–149.
- Bassot, J.-P., 1988. Apport de la télédétection à la compréhension de la géologie du Gabon. *Chron. Rech. Min.* 419, 25–34.
- Black, R., Liégeois, J.-P., 1993. Cratons, mobile belts, alkaline rocks and continental lithospheric mantle: the Pan-African testimony. *J. Geol. Soc. London* 150, 89–98.
- Boudzoumou, F., Trompette, R., 1988. La chaîne panafricaine ouest-congolienne au Congo (Afrique Equatoriale): un socle polycyclique charrié sur un domaine subautochtone formé par l’aulacogène du Mayombe et le bassin de l’Ouest-Congo. *Bull. Soc. Géol. France* 6, 889–896.
- Byamungu, B.R., Louis, P., Caby, R., 1987. Reconnaissance gravimétrique de la chaîne ouest-congolienne, Congo-Bas-Zaïre. *J. Afr. Earth Sci.* 6, 767–772.
- Cahen, L., 1978. La stratigraphie et la tectonique du Supergroupe Ouest-Congolien dans les zones médiane et externe de l’orogène Ouest-Congolien (Pan-Africain) au Bas-Zaïre et dans les régions voisines. *Ann. Mus. R. Afr. Centr., Tervuren (Belg.)*, in-8°, *Sci. Géol.* 83, p. 150.
- Cahen, L., Delhal, J., Ledent, D., 1976. Chronologie de l’orogénèse Ouest-Congolienne (pan-africaine) et comportement isotopique de roches d’alcalinité différente dans la zone interne de l’orogène au Bas-Zaïre. *Ann. Soc. Géol. Belg.* 99, 189–203.
- Cahen, L., Ledent, D., Tack, L., 1978. Données sur la géochronologie du Mayumbien (Bas-Zaïre). *Bull. Soc. Belg. Géol.* 87, 101–112.
- Cahen, L., Snelling, N.J., Delhal, J., Vail, J.R., 1984. *The Geochronology of Africa*. Clarendon Press, Oxford, p. 512.
- Campbell, I.H., Griffiths, R.W., 1990. Implications of mantle plume structure for the evolution of flood basalts. *Earth Planet. Sci. Lett.* 99, 79–93.
- Claué-Long, J.C., Compston, W., Roberts, J., Fanning, C.M., 1995. Two Carboniferous ages: a comparison of

- SHRIMP zircon ages with conventional zircon ages and $^{40}\text{Ar}/^{39}\text{Ar}$ analysis. In: Berggren, W.A., Kent, D.V., Aubrey, M.-P., Hardenbol, J. (Eds.), *Geochronology, Time Scales, and Global Stratigraphic Correlation*, S.E.P.M. Special Publication 54, pp. 3–21.
- Compston, W., Williams, I.S., Meyer, C., 1984. U–Pb geochronology of zircons from lunar breccia 73217 using a sensitive high mass-resolution ion microprobe. *J. Geophys. Res. Suppl.* 89, 525–534.
- Compston, W., Williams, I.S., Kirschvink, J.L., Zhang, Z.C., Ma, G.G., 1992. Zircon U–Pb ages for the Early Cambrian time-scale. *J. Geol. Soc. London* 149, 171–184.
- Cumming, G.L., Richards, J.R., 1975. Ore lead isotope ratios in a continuously changing Earth. *Earth Planet. Sci. Lett.* 28, 155–171.
- Dadot, P., 1966. Carte géologique de la République du Congo, échelle 1/500.000. Zone comprise entre les parallèles 2 et 5° Sud. Bureau de Recherches géologiques et minières (BRGM), France.
- Delhal, J., Ledent, D., 1976. Age et évolution comparée des gneiss migmatitiques prézadinien des régions de Boma et de Mpozo-Tombagadio (Bas-Zaïre). *Ann. Soc. Géol. Belg.* 99, 165–187.
- Delhal, J., Ledent, D., Pasteels, P., Venier, J., 1971. Etude du comportement isotopique de systèmes Rb/Sr et U/Pb dans le granite hyperalcalin de Noqui (Rép. Dém. Congo et Angola). *Ann. Soc. Géol. Belg.* 94, 223–236.
- de Araújo, A.G., Perevalov, O.V., 1998. Carta de Recursos Minerais, Escala 1/1000000. República de Angola, Ministério de Geologia e Minas, Instituto Geológico de Angola.
- de Araújo, A.G., Perevalov, O.V., Jukov, R.A., 1988. Carta geológica de Angola. Escala 1/1000000. República Popular de Angola, Ministério da Industria, Instituto Nacional de Geologia.
- de Carvalho, H., 1981. Geologia de Angola. Folha No 1. Escala 1/1000000. Laboratório Nacional de Investigação Científica Tropical, Junta de Investigações Científica do Ultramar.
- De Paepe, P., Hertogen, J., Tack, L., 1975. Mise en évidence de laves en coussin dans les faciès volcaniques basiques du massif de Kibungu (Bas-Zaïre) et implications pour le magmatisme ouest-congolien. *Ann. Soc. Géol. Belg.* 98, 251–270.
- Desthieux, F., 1992. Carte géologique de la République du Congo, 1/1000000. Ministère des Mines et de l'Énergie. Direction des Ressources minérales.
- Desthieux, F., 1994. Carte géologique de la République du Congo, 1/1000000. Nouvelle édition avec légende mise à jour. Ministère des Mines et de l'Énergie. Direction des Ressources minérales.
- Djama, L.M., Leterrier, J., Michard, A., 1992. Pb, Sr and Nd isotope study of the basement of the Mayumbian belt (Guena gneisses and Mfoubou granite, Congo): implications for crustal evolution in Central Africa. *J. Afr. Earth Sci.* 14, 227–237.
- Durrheim, R.J., Mooney, W.D., 1991. Archean and Proterozoic crustal evolution: evidence from crustal seismology. *Geology* 19, 606–609.
- Fernandez-Alonso, M., Deblond, A., Tack, L., 2000. The West Congolian (Pan-African) belt: an updated 1:1 million geological compilation map. Congress Program 31st International Geological Congress. Rio de Janeiro, Brazil, p. 146.
- Franssen, L., André, L., 1988. The Zadinian Group (late Proterozoic, Zaïre) and its bearing on the origin of the West-Congo orogenic belt. *Prec. Res.* 38, 215–234.
- Garland, F., Hawkesworth, C.J., Mantovani, S.M., 1995. Description and petrogenesis of the Paraná rhyolites, southern Brazil. *J. Petrology* 36, 1193–1227.
- Gresse, P., 1995. Transpression and transtension in the late Pan-African Vanrhynsdorp foreland thrust-fold belt, South-Africa. *J. Afr. Earth Sci.* 21, 91–105.
- Hartzer, F.J., 1998. A stratigraphic table of the SADC Countries. Council for Geoscience, South Africa.
- Hill, R.I., Campbell, I.H., Davies, G.F., Griffiths, R.W., 1992. Mantle plumes and continental tectonics. *Science* 256, 186–193.
- Hudeley, H., Belmonte, Y., 1966. Carte géologique de la République Gabonaise, échelle 1/1000000. Bureau de Recherches Géologiques et Minières (BRGM).
- Kampunzu, A.B., Kapenda, D., Manteka, B., 1991. Basic magmatism and geotectonic evolution of the Pan-African belt in central Africa: evidence from the Katangan and West Congolian segments. *Tectonophysics* 190, 363–371.
- Kirstein, L.A., Peat, D.W., Hawkesworth, C.J., Turner, S.P., Harris, C., Mantovani, M.S.M., 2000. Early Cretaceous basaltic and rhyolitic magmatism in southern Uruguay associated with the opening of the South Atlantic. *J. Petrology* 41, 1413–1438.
- Korpershoek, H.R., 1964a. The geology of degree sheet sul B33/H-N (Noqui-Tomboco). Part 1. *Bol. Serv. Min. Angola* 9, 5–183.
- Korpershoek, H.R., 1964b. The geology of degree sheet sul B33/H-N (Noqui-Tomboco). Part 2. *Bol. Serv. Min. Angola* 10, 9–106.
- Lepersonne, J., 1969. Etude photogéologique de la région de Matadi. Rapport Annuel 1968 du Département de Géologie et Minéralogie, Mus. R. Afr. Centr., Tervuren (Belg.), pp. 29–33.
- Lepersonne, J., 1974. Carte géologique du Zaïre au 1/2000000 et notice explicative. République du Zaïre, Département des Mines, Direction de la Géologie, p. 67.
- Lightfoot, P.C., Hawkesworth, C.J., Sethna, S.F., 1987. Petrogenesis of rhyolites and trachytes from the Deccan trap: Sr, Nd and Pb isotope and trace element evidence. *Contrib. Min. Petrology* 95, 44–54.
- Ludwig, K.R., 1999. Using Isoplot/Ex Version 2.01, A Geochronological Toolkit for Microsoft Excel: Berkeley Geochronology Center Special Publication 1a, p. 47.
- Luttinen, A.B., Furnes, H., 2000. Flood basalts of Vestfjella: Jurassic magnetism across an Archaean–Proterozoic lithospheric boundary in Dronning Maud Land, Antarctica. *J. Petrology* 41, 1271–1305.
- Maurin, J.-C., 1993. La chaîne panafricaine ouest-congolienne: corrélation avec le domaine est-brésilien et hypothèse géodynamique. *Bull. Soc. Géol. France* 764, 51–60.

- Maurin, J.-C., Mpemba-Boni, J., Pin, C., Vicat, J.-P., 1990. La granodiorite de Les Saras, un témoin de magmatisme éburnéen (2 Ga.) au sein de la chaîne ouest-congolienne: conséquences géodynamiques. *C.R. Acad. Sci. Paris* 310, 571–575.
- Maurin, J.-C., Boudzoumou, F., Djama, L.-M., Gioan, P., Michard, A., Mpemba-Boni, J., Peucat, J.-J., Pin, C., Vicat, J.-P., 1991. La chaîne protérozoïque ouest-congolienne et son avant-pays au Congo: nouvelles données géochronologiques et structurales, implications en Afrique centrale. *C.R. Acad. Sci. Paris* 312, 1327–1334.
- Molina, E.C., Ussami, N., 1999. The geoid in southeastern Brazil and adjacent regions: new constraints on density distribution and thermal state of the lithosphere. *J. Geodyn.* 28, 357–374.
- Mpemba Boni, J., Vellutini, P.J., 1992. Caractérisation géochimique des dykes basiques du massif de les Saras (Mayombe Congolais, Afrique Centrale): conséquences géodynamiques. *J. Afr. Earth Sci.* 14, 209–215.
- Namegabe, M.R., 1981. Analyse par activation neutronique des laves du volcan Nyiragongo (Kivu/Zaire) et des séquences précambriennes du Bas-Zaire. Unpublished Ph.D. thesis, Rijksuniversiteit Gent, p. 218.
- Navez, J., 1995. Détermination d'éléments en traces dans les roches silicatées par ICP-MS. Rapport Annuel 1993–1994 du Département de Géologie et Minéralogie, Mus. R. Afr. Centr., Tervuren (Belg.), pp. 139–147.
- Nelson, B.K., De Paolo, D.J., 1985. Rapid production of continental crust 1.7–1.9 billion year ago: Nd isotopic evidence from the basement of the North American mid-continent. *Geol. Soc. Am. Bull.* 96, 746–754.
- Pearce, J.A., 1983. Role of the sub-continental lithosphere in magma genesis at active continental margins. In: Hawkesworth, C.J., Norry, M.J. (Eds.), *Continental Basalts and Mantle Xenoliths* Shiva Geology Series. Nantwich, UK, pp. 230–249.
- Pedrosa-Soares, A.C., Noce, C.M., Vidal, P., Monteiro, R., Leonardos, O., 1992. Toward a new tectonic model for the Late Proterozoic Araçuaí (SE Brazil)–West Congolian (SW Africa) Belt. *J. S. Am. Earth Sci.* 6, 33–47.
- Pedrosa-Soares, A.C., Vidal, P., Leonardos, O.H., de Brito-Neves, B.B., 1998. Neoproterozoic oceanic remnants in Eastern Brazil: further evidence and refutation of an exclusively ensialic evolution for the Araçuaí–West Congo orogen. *Geology* 26, 519–522.
- Pedrosa-Soares, A.C., Noce, C.M., Wiedemann, C., Pinto, C.P., 2001. The Araçuaí–West-Congo Orogen in Brazil: an overview of a refined orogen formed during Gondwanaland assembly. *Prec. Res.*, 110, 307–323.
- Pidgeon, R.T., Furfaro, D., Kennedy, A.K., Nemchin, A.A., Van Bronswijk, W., 1994. Calibration of zircon standards for the Curtin SHRIMP II. Abstracts of the Eighth International Conference on Geochronology, Cosmochronology and Isotope Geology. Berkeley, USA, US Geological Survey, Circular 1107, p. 251.
- Porada, H., Berhorst, V., 2000. Towards a new understanding of the Neoproterozoic–Early Palaeozoic Lufilian and northern Zambezi belts in Zambia and the Democratic Republic of Congo. *J. Afr. Earth Sci.* 30, 727–771.
- Sambridge, M.S., Compston, W., 1994. Mixture modelling of multi-component data sets with application to ion-probe zircon ages. *Earth Planet. Sci. Lett.* 128, 373–390.
- Sheth, H.C., 1999. A historical approach to continental flood basalt volcanism: insight into pre-volcanic rifting, sedimentation, and early alkaline magmatism. *Earth Planet. Sci. Lett.* 168, 19–26.
- Steenstra, B., 1973. Etat des connaissances sur la stratigraphie du 'Zadinien' dans le Bas-Zaire. Rapport Annuel 1972 du Département de Géologie et Minéralogie, Mus. R. Afr. Centr., Tervuren (Belg.), pp. 70–81.
- Steiger, R.H., Jäger, E., 1977. Subcommission on geochronology: convention on the use of decay constants in geo- and cosmo-chronology. *Earth Planet. Sci. Lett.* 36, 359–362.
- Tack, L., 1973a. Le massif de la Lufu et sa bordure (Rép. du Zaire), note préliminaire. *Ann. Soc. Géol. Belg.* 96, 31–48.
- Tack, L., 1973b. Le massif de Yoyo et sa bordure (Rép. du Zaire), note préliminaire. *Ann. Soc. Géol. Belg.* 96, 49–54.
- Tack, L., 1975a. Bijdrage tot de studie van de geologie, de petrografie en de petrologie van het Mayumbiaan van Neder-Zaire. Unpublished Ph.D. thesis, Rijksuniversiteit Gent (Belgium), p. 200, + annexes.
- Tack, L., 1975b. Etude pétrochimique de la Formation des Roches vertes de la région d'Inga au Bas-Zaire. *Ann. Soc. Géol. Belg.* 98, 229–249.
- Tack, L., 1979a. Etude pétrochimique du Mayumbien au Bas-Zaire: une séquence volcano-plutonique acide précambrienne. *Ann. Mus. R. Afr. Centr., Tervuren (Belg.)*, in-8°, *Sci. Géol.* 84, p. 56.
- Tack, L., 1979b. Données pétrochimiques concernant les roches vertes de la région d'Inga au Bas-Zaire. *Ann. Soc. Géol. Belg.* 102, 181–184.
- Tack, L., 1979c. Données pétrochimiques concernant des roches vertes affleurant dans la région de Bibuanga au Mayumbe (Bas-Zaire). *Ann. Soc. Géol. Belg.* 102, 185–187.
- Tack, L., 1983. Extension du Mayumbien au Bas-Zaire: le problème de sa délimitation cartographique et implications sur les concepts du cadre géologique général du Précambrien du Bas-Zaire. Rapport Annuel 1981–1982 du Département de Géologie et Minéralogie, Mus. R. Afr. Centr., Tervuren (Belg.), pp. 127–133.
- Tack, L., 1995. The West Congolian (Pan-African) Belt: an updated synthesis. *Soc. géol. France, séance spécialisée 'Géodynamique du Paléoproterozoïque'*, Orléans, France, Abstracts volume, 35.
- Tack, L., Fernandez-Alonso, M., 1998. The West Congolian belt: a critical assessment of available time constraints during the Neoproterozoic and Palaeozoic amalgamation of Gondwana. Special abstracts issue. *Gondwana 10: event stratigraphy of Gondwana*. *J. Afr. Earth Sci.* 27, 193.
- Taylor, S.R., McLennan, S.M., 1985. *The Continental Crust: Its Composition and Evolution*. Blackwell, Oxford, UK, p. 312.

- Thirlwall, M.F., Upton, B.J.G., Jenkins, C., 1994. Interaction between continental lithosphere and the Iceland plume — Sr–Nd–Pb isotope geochemistry of Tertiary basalts, NE Greenland. *J. Petrology*, 35, 839–879.
- Thompson, R.N., Morrison, M.A., Dickin, A.P., Hendry, G.L., 1983. Continental flood basalts ... arachnids rule OK? In: Hawkesworth, C.J., Norry, M.J. (Eds.), *Continental Basalts and Mantle Xenoliths Shiva Geology Series*, Nantwich, UK, pp. 158–187.
- Trompette, R., 1994. *Geology of Western Gondwana (2000–500 Ma). Pan-African-Brasiliano Aggregation of South America and Africa*. Balkema, Rotterdam, The Netherlands, p. 350.
- Trompette, R., 2000. Gondwana evolution; its assembly at around 600 Ma. *C.R. Acad. Sci. Paris, Sci. Terre et des planètes/Earth Planetary Sci. Geodyn./Géodyn.* 330, 305–315.
- Turner, S., Hawkesworth, C., 1995. The nature of the sub-continental mantle: constraints from the major-element composition of continental flood basalts. *Chem. Geol.* 120, 295–314.
- Unrug, R., 1996. The assembly of Gondwanaland. Scientific results of IGCP Project 288: Gondwanaland sutures and mobile belts. *Episodes* 19, 11–20.
- Unrug, R., 1997. Rodinia to Gondwana: the Geodynamic map of Gondwana Supercontinent Assembly. *GSA Today* 7, 1–6.
- Unrug, R., Castaing, C., Feybesse, J.-L., Gresse, P.G., Powell, C.M., Sadowski, G.R., Tack, L., 1996. Geodynamic Map of Gondwana Supercontinent Assembly. IGCP Project 288: Gondwanaland Sutures and Fold Belts. Council for Geoscience, Pretoria, South Africa and Bureau Recherches Géologiques Minières (BRGM), Orléans, France, 4 sheets.
- Vellutini, P.J., Rocci, G., Vicat, J.-P., Cioan, P., 1983. Mise en évidence de complexes ophiolitiques dans la chaîne du Mayombe (Gabon–Angola) et nouvelle interprétation géotectonique. *Prec. Res.* 22, 1–21.
- Vicat, J.-P., Vellutini, P.J., 1987. Sur l'origine océanique des metabasites de la chaîne du Mayombe (Gabon, Congo, Zaïre, Angola). *Prec. Res.* 36, 163–175.
- Vicat, J.-P., Vellutini, P.J., 1988. Géologie et géochimie de la série précambrienne de la Bikossi, le long du réalignement du chemin de fer congo-océan, dans la chaîne du Mayombe (République populaire du Congo). *J. Afr. Earth Sci.* 7, 811–820.
- Vicat, J.-P., Maurin, J.-C., Djama, L.M., Léger, J.-M., 1992. Les granites à étain, datés à 1 Ga de la chaîne Ouest-Congolienne (République Populaire du Congo): géochimie et implications géodynamiques en Afrique Centrale. *IGCP no. 255. Bulletin/Newsletter* 4, 61–65.